

# Large Models are Parsimonious Learners: Activation Sparsity in Trained Transformers

Zonglin Li\*, Chong You\*, Srinadh Bhojanapalli, Daliang Li, Ankit Singh Rawat, Sashank J. Reddi, Ke Ye, Felix Chern, Felix Yu, Ruiqi Guo, and Sanjiv Kumar

Google Research, New York City

October 13, 2022

## Abstract

This paper studies the curious phenomenon for machine learning models with Transformer architectures that their activation maps are *sparse*. By activation map we refer to the intermediate output of the multi-layer perceptrons (MLPs) after a ReLU activation function, and by “sparse” we mean that on average very few entries (e.g., 3.0% for T5-Base and 6.3% for ViT-B16) are nonzero for each input to MLP. Moreover, larger Transformers with more layers and wider MLP hidden dimensions are sparser as measured by the percentage of nonzero entries. Through extensive experiments we demonstrate that the emergence of sparsity is a prevalent phenomenon that occurs for both natural language processing and vision tasks, on both training and evaluation data, for Transformers of various configurations, at layers of all depth levels, as well as for other architectures including MLP-mixers and 2-layer MLPs. We show that sparsity also emerges using training datasets with random labels, or with random inputs, or with infinite amount of data, demonstrating that sparsity is not a result of a specific family of datasets. We discuss how sparsity immediately implies a way to significantly reduce the FLOP count and improve efficiency for Transformers. Moreover, we demonstrate perhaps surprisingly that enforcing an even sparser activation via Top- $k$  thresholding with a small value of  $k$  brings a collection of desired but missing properties for Transformers, namely less sensitivity to noisy training data, more robustness to input corruptions, and better calibration for their prediction confidence.

## 1 Introduction

The great success of modern machine learning for applications in computer vision, natural language processing, game playing, and beyond is driven primarily by the computational model known as deep neural networks (DNNs) [1]. With inspirations drawn from information processing in biological brains, DNNs are *artificial* neural networks constructed from distributed computational nodes (a.k.a. neurons) with inter-connections learned from data. Compared to shallow machine learning models, DNNs possess superior learning capacity and hence can handle complex real-world tasks.

Although motivated from biological brains, there are differences at very fundamental levels on how artificial and biological neural networks work. One of such differences is in the sparsity of computation. Evidence from neuroscience suggests that neural activity in biological brains is *sparse*, namely, only a small percentage of all neurons fire at each time [2, 3, 4, 5]. Sparse firing suggests that despite having billions of neurons, only a small fraction of the brain participates in computation at each time. This may explain why brains can sustain at a very low energy cost. In contrast, learning and inference with DNNs rely primarily on dense computations where all neurons are involved for any input. In fact, modern computational hardware for deep neural networks, such as GPUs and TPUs, are designed to facilitate massive scale dense computations. Even with such dedicated hardware, DNNs are still notoriously resource-demanding to train and deploy. Aside from computation efficiency, artificial neural networks also lag far behind biological ones in terms of robustness to input perturbation, error correction for erroneous training labels, confidence calibration for the predictions, etc.

---

\*Equal contribution

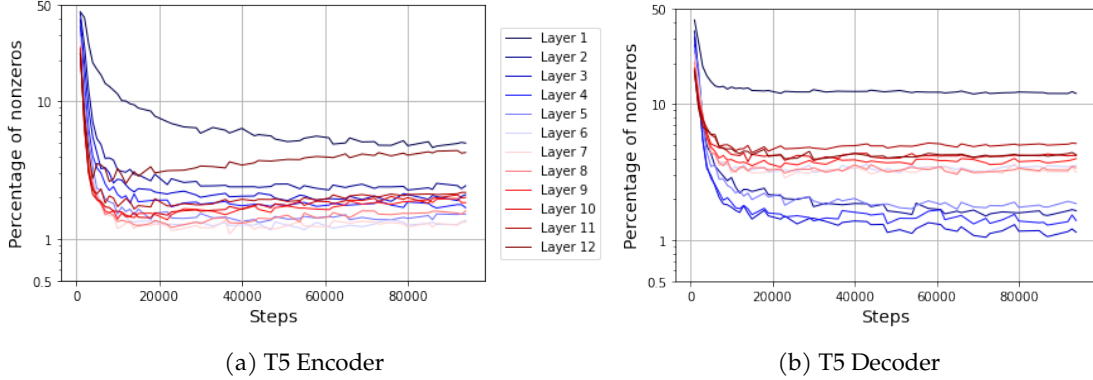


Figure 1: Percentage of nonzero entries (y-axis, log scale) in the activation map as a function of number of training steps (x-axis) for a T5-Base model trained with the span corruption objective on the C4 dataset. **Left:** layers (from shallow to deep) of the encoder. **Right:** layers of the decoder.

## 1.1 An Intriguing Observation: Activations are *Sparse* in Trained Transformers

This paper provides an extensive study on a surprising observation that despite performing dense computations, DNNs produce very *sparse* activation in its intermediate layers once trained<sup>1</sup>. Specifically, we study *Transformer* [6], a DNN model architecture that has become a workhorse for modern applications. Transformers are constructed from interweaving a self-attention module and a multi-layer perceptrons (MLPs) of depth 2, and the focus of this paper is on the activation map in the intermediate output of MLPs (after the activation function). Figure 1 shows the sparsity of the activation maps, measured by the percentage of nonzeros, in all MLP layers of a T5-Base model which is a Transformer based encoder-decoder model for natural language processing [7]. We see that the percentage of nonzero entries is around 50% at initialization, which is expected: randomly initialized weights produce roughly equal numbers of positive and negative entries in the pre-activation map, resulting in  $\sim 50\%$  non-zeros after the ReLU. However, at the end of training the percentage of nonzero entries reduces drastically: the average value across all encoder-decoder layers is 2.7% with the largest one being 12.0% and the smallest one being only 1.1%. The emergence of sparse activation in Transformers bears a similarity to the sparsity of neural activities in biological brains, revealing an interesting connection between artificial and biological neural networks. Moreover, unlike classical sparse methods where such a connection is established via *explicit* sparse regularization [8], the sparsity observed in Transformers is emergent without any explicit design.

It is worth noting that the observation that Transformers produce sparse activations is previously reported in [9]. Our paper significantly extends upon results in [9] to demonstrate that sparsity emerges prevalently at all layers of Transformers, for both language and vision tasks, on both training and evaluation data, and for some architectures beyond Transformers. We also examine the activation of individual neurons, to show that sparsity is not caused by “dead” neurons and that the percentage of activation has a long tail distribution. In addition, by experiments with particularly designed datasets, as well as theoretical analysis of gradient at the beginning of training, we show that the emergence of sparsity may be due to the training dynamics rather than particular choices of datasets. Finally, our paper provides empirical evidence that sparsity is positively correlated with model robustness and calibration.

## 1.2 Prevalence, Causes, and Benefits of Sparsity

This paper provides a study on the aforementioned phenomenon of sparse activation in trained Transformer models, with a focus on answering the following three questions. First, is the phenomenon in Figure 1 a corner case or is it occurring more broadly? Second, what are the causes for the emergence of sparsity? Third, why should we care about the sparsity in DNNs, other than the appeal of its similarity to biological brains? Our main results along these lines are summarized below.

<sup>1</sup>This implies, as we explain in details later, that a lot of the computations are spent in vain with multiplying a value by zero.

1. **Sparsity is a prevalent phenomenon.** We show in Section 2 that the emergence of sparsity in activation maps of T5 as reported in Figure 1 is not an isolated and cherry-picked case. Rather, sparsity is prevalent, and occurs broadly in Transformer models: it emerges in all layers of a Transformer, for Transformers trained on both vision and natural language data, for Transformers of various configurations, and for activation maps computed on both training and test data, etc. Moreover, through controlled experiments on the width and depth of Transformers, we reveal that larger models are sparser, as measured by percentage of nonzero entries. We also show in Appendix B.1 that sparsity emerge in MLP-Mixers, vanilla MLPs, and to some extent convolutional neural networks.
2. **Sparsity comes from training dynamic?** Towards understanding where sparsity comes from, one argument is that commonly used image and natural language training datasets entail a compact representation due to information in the labels or intrinsic low-dimensional structures of the natural data. Another hypothesis is that sparsity has nothing to do with commonly used training datasets, and arises as a result of modern over-parameterized models being able to fit the training data even when it is generated in random. In Section 3, we design experiments using training datasets with random labels, or random images, or infinitely amount of data, to show that none of the above fully explains the emergence of sparsity. Based on our observations, we speculate that the sparsity may be attributed to the training dynamic in the optimization process. In particular, we show theoretically with a simplified model architecture that the descending direction of gradient at the beginning of training points to decreasing the value of activations.
3. **Sparsity improves efficiency, robustness, and calibration.** Sparsity of activation map implies that a lot of the computations being carried out in model training and inference is wasted: they are doing nothing but multiplying some value by zero. This immediately suggests a trivial way of reducing the FLOPs via avoiding all such computations, which we discuss in Section 4.1. Importantly, this simple strategy does not affect model output hence their performance at all, which is in contrast to existing work for improving efficiency via sparsity that is built upon trial-and-error without ensuring their correctness [10]. To explicitly control the sparsity level, we further introduce *Top- $k$  Transformer* in Section 4.2, a simple modification of Transformers where a Top- $k$  thresholding is applied to the activation maps<sup>2</sup>. We provide experimental evidence that reduction in FLOPs via sparsity brings wall time benefits for unbatched decoding on TPUs with Top- $k$  T5 models with 11B parameters.

While it is straightforward to associate sparsity with computational efficiency, it may be less obvious and somewhat surprising that sparsity is associated with reliability of the models as well. We show in Section 4.3 that enforcing explicit sparsity via Top- $k$  Transformers improves model performance in terms of less sensitivity to noisy training data, less sensitivity to input corruptions, and better confidence calibration.

### 1.3 Experimental Setup

We study the sparsity in activation maps of Transformers with two commonly used Transformer models, namely Text-to-Text Transfer Transformer (i.e., T5) and Vision Transformer (i.e., ViT).

- T5 is an encoder-decoder model for natural language processing tasks [7]. We train T5 on the Colossal Clean Crawled Corpus (C4) using the span corruption task as suggested by [7].
- ViT is an encoder model for vision tasks [13]. Unless specified otherwise, we train ViT on ImageNet-21k [14], an image classification dataset with 14M images and 21k classes. For certain cases we also use ImageNet-1k which is a subset of ImageNet-21k with 1.3M images and 1k classes.

Beyond T5 and ViT, we also present the results for BERT in the Appendix.

We measure the sparsity level at the intermediate output of the two-layer MLPs in a Transformer. Recall that an MLP performs the following mapping

$$f(\mathbf{x}; \mathbf{K}, \mathbf{V}) \doteq \sum_{i=1}^{d_{\text{ff}}} \left( \sigma(\langle \mathbf{k}_i, \mathbf{x} \rangle) \cdot \mathbf{v}_i \right), \text{ or equivalently, } f(\mathbf{x}; \mathbf{K}, \mathbf{V}) \doteq \mathbf{V} \sigma(\mathbf{K}^\top \mathbf{x}), \quad (1)$$

where  $\mathbf{x} \in \mathbb{R}^{d_{\text{model}}}$  is the input,  $\mathbf{K} = [\mathbf{k}_1, \dots, \mathbf{k}_{d_{\text{ff}}}] \in \mathbb{R}^{d_{\text{model}} \times d_{\text{ff}}}$  and  $\mathbf{V} = [\mathbf{v}_1, \dots, \mathbf{v}_{d_{\text{ff}}}] \in \mathbb{R}^{d_{\text{model}} \times d_{\text{ff}}}$  are learnable layer parameters, and  $\sigma()$  is a nonlinear activation function. We use ReLU as the activation function  $\sigma()$  for

<sup>2</sup>The approach is previously adopted in ConvNets for improving model robustness [11], and more recently in [12] for improving memory efficiency of Transformers.

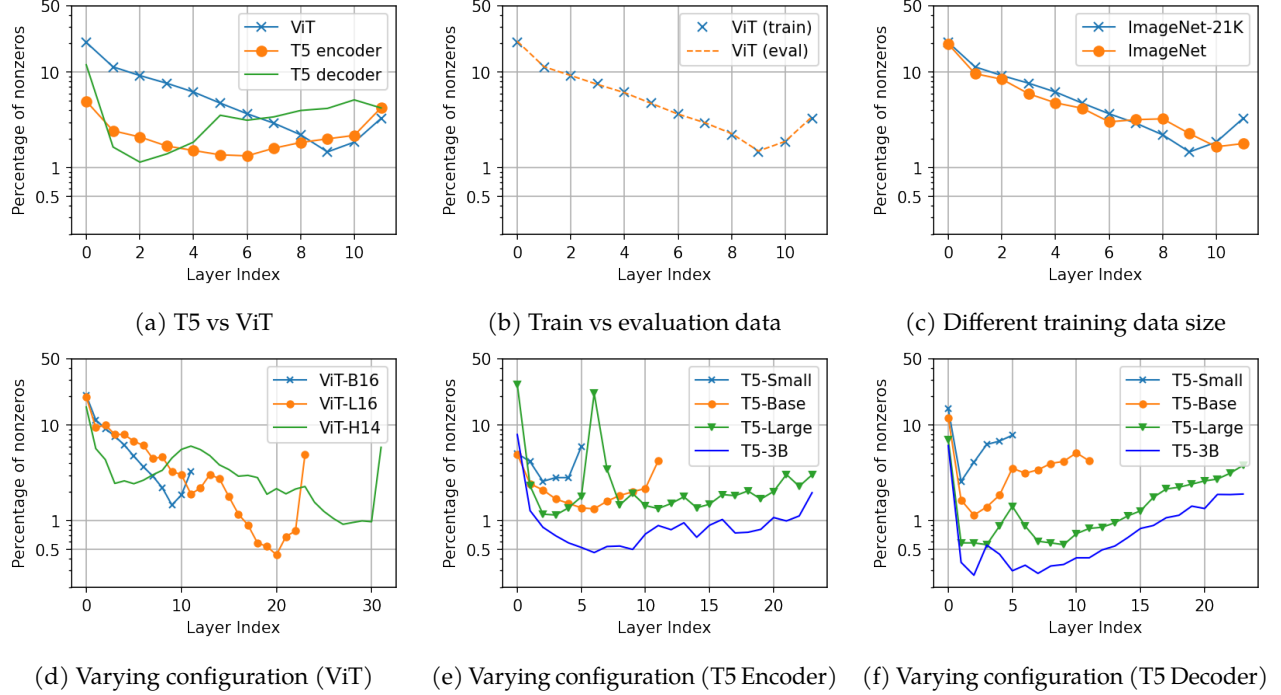


Figure 2: Percentage of nonzero entries across different layers of trained Transformers (a) for both language data with T5 and vision data with ViT, (b) on both training and evaluation data, (c) for ViT trained on two ImageNet of different scales (21k vs 1k classes), (d) on ViT of varying configurations, and (e, f) on T5 of varying configurations. Please note that the y-axis is in log scale. *Sparsity emerges in all cases.*

both T5 and ViT<sup>3</sup>. A two-layer MLP may be regarded as having  $d_{\text{ff}}$  neurons where the  $i$ -th neuron performs the computation  $\sigma(\langle \mathbf{k}_i, \mathbf{x} \rangle) \cdot \mathbf{v}_i$ , and the final layer output is the sum of the output of all neurons. Each neuron is called *activated* if  $\sigma(\langle \mathbf{k}_i, \mathbf{x} \rangle)$  is strictly positive. Hence, the sparsity of neuron activation can be measured by the number of nonzero entries in the feature map

$$\mathbf{a} \doteq \sigma(\mathbf{K}^\top \mathbf{x}), \quad (2)$$

which is a vector of dimension  $d_{\text{ff}}$ .

Both T5 and ViT come with several configurations for  $d_{\text{model}}$ ,  $d_{\text{ff}}$ , number of layers, etc. Unless specified otherwise, we will use the Base models (i.e., T5-Base and ViT-B/16) which have  $d_{\text{model}} = 768$ ,  $d_{\text{ff}} = 3072$ , and 12 layers (for ViT) and 12 encoder layers + 12 decoder layers (for T5). Training details of T5 and ViT are provided in Appendix A.

## 2 Prevalence of Sparsity in Learned Transformers

This section shows thorough experiments on commonly used Transformers that sparsity in activation maps is a prevalent phenomenon. We also show through some controlled experiments that deeper and wider Transformers tend to be sparser measured by percentage of nonzero entries in activation maps.

### 2.1 Sparsity is a Ubiquitous Phenomenon

We start by providing experimental evidence that the emergence of sparse activation in trained Transformers is a ubiquitous phenomenon. To this end, we plot the percentage of nonzero entries of activation maps in different Transformers, and present the results in Figure 2. Such results demonstrate the following.

<sup>3</sup>ViT originally uses GeLU as its activation function as in [13]. Here we switch to using ReLU as it allows us to more easily measure the sparsity level using the number of nonzero entries.

- *Sparsity emerges for both Vision and NLP tasks.* Figure 2a shows the percentage of nonzero entries of trained T5 and ViT models evaluated on their respective training datasets. We see that both encoder and decoder of T5, as well as the ViT, all exhibit sparsity.
- *Sparsity emerges on both training and evaluation data.* Figure 2b shows the percentage of nonzero entries in a trained T5 evaluated on both the training data and the evaluation data. We see that the property of sparsity generalizes very well to evaluation data as the curves for training and evaluation data align very closely with each other.
- *Sparsity emerges on datasets of varying scale.* Figure 2c shows the percentage of nonzero entries in ViT trained on both ImageNet-21k and ImageNet-1k, where the former is a superset of the latter with approximately  $10\times$  more images and  $21\times$  more classes. We see that the scale of data does not affect much of the sparsity level.
- *Sparsity emerges on Transformers of varying configurations.* Figure 2d shows the percentage of nonzero entries for ViT of varying configurations in model size. Figure 2e and 2f show the percentage of nonzero entries for encoder and decoder, respectively, of T5 with varying configurations in model size. We see that sparsity persists for all cases.
- *Sparsity emerges across all layers of a Transformer.* Finally, all plots in Figure 2 show that sparsity emerges in all layers of a Transformer. Moreover, in all cases the first few and last few layers tend to be denser than intermediate layers.

The presence of sparsity in activation maps does not rule out the possibility that a small percentage of the neurons are always activated for all inputs, whereas the rest of the neurons are never activated. To illustrate that this is not the case, we experiment with a pretrained T5 base model<sup>4</sup> to plot the percentage of layer inputs for which each of the  $d_{\text{ff}}$  neurons is activated when evaluated on 800 examples taken from C4 dataset with span corruption task. Note that there are  $800 * 512 = 409600$  samples as MLP activation is computed per token. The results are presented in Figure 3 with x-axis being indices of neurons in the first encoder layer of T5 sorted in descending order according to percentage of layer inputs on which they are activated. It can be seen that while a few neurons are activated for around 50% of the time, the vast majority of neurons (around 93.5%) are activated less than 10% of the time. Moreover, there are no dead neurons that are never activated, and the least activated neuron is activated for around 0.001% of the time, and 99% of neurons are activated over 1% of the time. Finally, while the results here are for neurons in the first MLP layer of a pretrained T5 base encoder, all other MLP layers show qualitatively similar behavior.

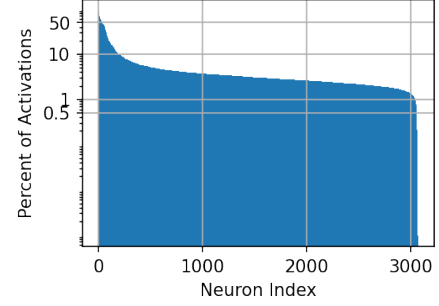


Figure 3: Percentage of times that each neuron in the first MLP layer of a trained T5 is activated on C4 dataset. 0.001% of the time, and 99% of neurons are activated over 1% of the time. Finally, while the results here are for neurons in the first MLP layer of a pretrained T5 base encoder, all other MLP layers show qualitatively similar behavior.

## 2.2 The Larger, the Sparser

We next examine the effect of model size on the sparsity level of activation maps. Note that Figure 2e and Figure 2f provide evidence with T5 of varying configuration that larger models tend to be sparser. Here we perform controlled experiments to examine the effect of model depth, measured by the number of Transformer layers, as well as the effect of model width, measured by the dimension of activation map of MLPs (i.e.,  $d_{\text{ff}}$ ), separately. Towards that, we take a standard T5 model and vary the depth and width, respectively while keeping the rest of the configuration fixed, and examine their sparsity level after training. The results are presented in Figure 4 for the encoder, whereas we omit the results for the decoder as they are qualitatively the same as those for encoder.

It can be seen from Figure 4a that deeper Transformers are arguably sparser. For example, many of the middle layers of the 32-layer model have less than 1% nonzero entries while all shallower models have more than 1% nonzero entries across all layers. For comparing networks of different widths, we measure the sparsity with the percentage and the count of nonzero entries in Figure 4b and Figure 4c, respectively. It can be seen that wider models have a lower percentage of nonzero entries, though a higher count of nonzero entries.

<sup>4</sup><https://github.com/google-research/t5x/blob/main/docs/models.md#t5-checkpoints>

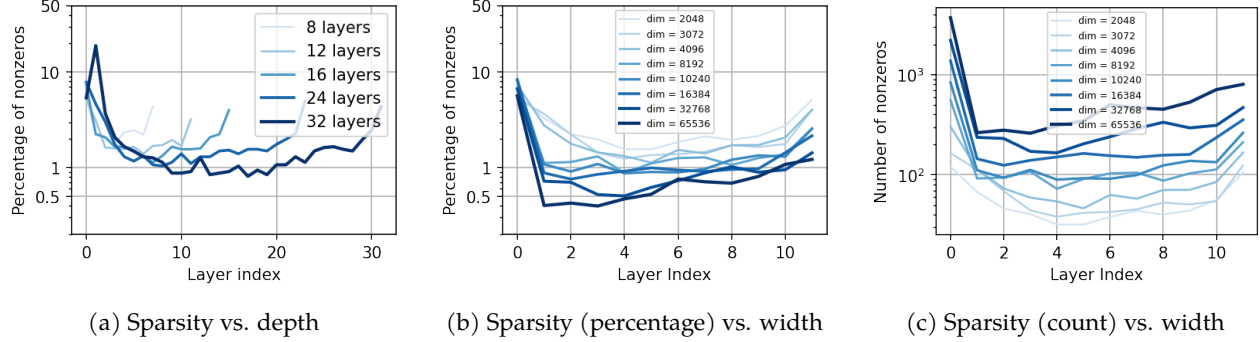


Figure 4: Activation sparsity across different encoder layers of trained T5 Transformers of (a) varying depth and (b, c) varying width. Since with varying width the dimension of activation maps also changes, we evaluate sparsity both in term of the percentage (as in (b)) and the count (as in (c)) of nonzeros. *Deeper and wider models are sparser in terms of percentage of activated neurons.*

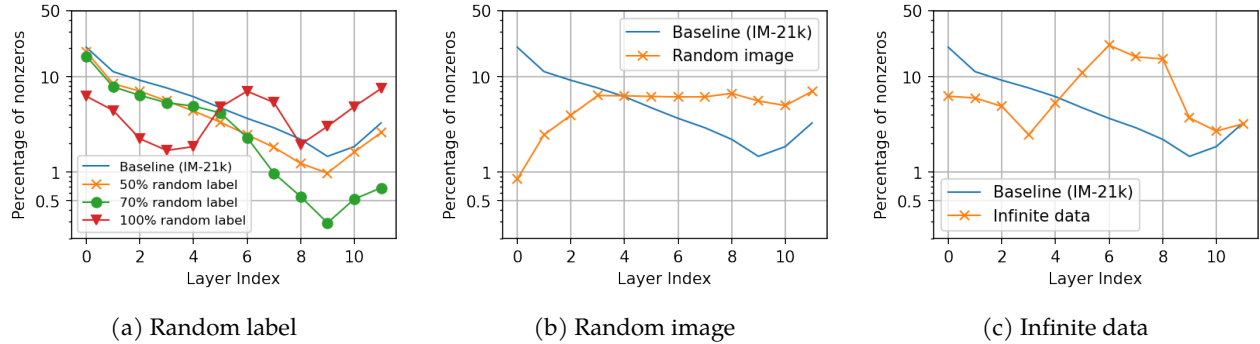


Figure 5: Percentage of nonzero entries in ViT trained on ImageNet-21k (IM-21K) with (a) *random labels* where  $p\%$  labels are replaced by labels drawn from a uniform distribution with  $p \in \{50\%, 70\%, 100\%\}$ , (b) *random images* where each image is replaced by one where the pixels are drawn from i.i.d. uniform distribution in  $[-1, 1]$ , and (c) *infinite data* where sufficient training data is generated by drawing random image and random label pairs so that the model is never trained on the same pair twice.

### 3 Sparsity from Training Dynamic?

In this section we study the causes of sparsity in activation maps of trained Transformers. Towards that, in Section 3.1, 3.2, and 3.3, we present a set of hypotheses and design corresponding experiments to validate or disprove them. We discuss the observation from the experiments and draw a tentative conclusion in Section 3.4 on attributing sparsity to the training dynamic, with theoretical evidence.

#### 3.1 Sparsity from Labels?

Transformers are usually trained via supervised learning (e.g., using the ImageNet dataset for ViT) or self-supervised learning (e.g., using the span corruption task for T5). In both cases, the training labels provide a pertinent and meaningful description of the corresponding training data (e.g., image for ViT and text for T5). Sparsity may arise because the label set provides a structured organization of the massive training data, hence the training dataset admits a compact representation. This motivates us to formulate the following hypothesis.

**Hypothesis 3.1** (Sparsity from labels). *Sparsity in trained Transformers arises from the labels for Transformer training, e.g., human annotations in supervised training or generated labels from data itself in self-supervised learning.*

We use a *random label* experiment with ViT for image classification to test Hypothesis 3.1. Specifically, we generate a new training dataset by replacing  $p\%$  of the labels in the ImageNet-21k dataset with random labels

drawn uniformly at random from the set of all possible labels, where  $p$  is varied to examine the effects. With such a dataset, the labels for a certain percentage of images do not provide a meaningful description for the content of the image. Hence, if Hypothesis 3.1 is valid, then the activation map will become dense.

The sparsity level of ViT trained on the random label datasets is shown in Figure 5a. It can be seen that the percentage of activated neurons decreases with an increasing percentage of label noise up to 70%. An even higher label noise level at 100% changes the sparsity level across layers as the shallow layers (i.e., layers 0 - 4) becomes sparser, while the deep layers (i.e., layers 5 - 11) becomes denser. Nonetheless, even with 100% label noise, all layers have  $< 10\%$  activated neurons.

### 3.2 Sparsity from Data?

While modern image and text data are often of high-dimensional, their intrinsic degree of freedom is much smaller, i.e., they are low-dimensional and admit compact representations [15, 16]. Hence, even if the labels do not provide meaningful descriptions of the data, it may still be possible that Transformers extract low-dimensional structures from data and produce compact representations in the form of sparse activation maps. This motivates the following hypothesis.

**Hypothesis 3.2** (Sparsity from natural data). *Sparsity in trained Transformers arises from natural training data (e.g., images for ViT and texts for T5).*

We use a *random image* experiment to test Hypothesis 3.2. With the ImageNet-21k dataset, we replace each image with a random image generated by drawing pixel values from an i.i.d. Uniform distribution in the range of [0, 255], and use these images (instead of the original images in ImageNet-21k) for model training. Such random images do not contain any low-dimensional structures nor compact representations.

The percentage of nonzero entries of a ViT trained on random image dataset is shown in Figure 5b. It can be seen that the first four layers become sparser while the last few layers become relatively denser compared to training with natural images in ImageNet-21k. Nonetheless, all layers have  $< 10\%$  activated neurons.

### 3.3 Sparsity from Data-fitting?

Modern deep neural networks are often *over-parameterized*, with sufficient capacity to fit practical training datasets and obtain close-to-zero training error. There is evidence suggesting that this result holds true even if the data and label are generated in random [17]. Hence, there is the possibility that sparsity arises because the training data, even if generated in random, is scarce relative to the scale of modern over-parameterized models.

**Hypothesis 3.3** (Sparsity from data-fitting). *Sparsity in trained Transformers arises from the fact that models have more than sufficient capacity to fit training data of practical scale.*

To test Hypothesis 3.3, we design an *infinite data* experiment where the amount of training data is infinitely large so that any practical Transformer becomes under-parameterized relative to the data and cannot fit the data. The way we generate infinite training data is to sample images with random pixels as in the random image experiment, and for each image we sample a random label as in the random label experiment. Moreover, we generate sufficient amount of such training data to make sure that the model never sees the same data point twice during the training. The number of training iterations in the infinite data experiment is kept the same as that of the random image and random label experiments.

The result of this experiment is presented in Figure 5c. It can be seen that the first four layers produce sparser activation maps, while middle layers with index 4 - 7 are considerably denser compared to the baseline with near 10% to 20% nonzero entries.

### 3.4 Discussion: Sparsity from Training Dynamic?

The results of random label, random image, and infinite data experiments in Figure 5 show that labels, data, and data-fitting as conjectured in Hypothesis 3.1, 3.2, and 3.3, respectively, all affect the sparsity level of the activation map. Nonetheless, none of them fully explains the emergence of sparsity since for all results in Figure 5, the percentage of nonzero entries is considerably smaller than at the initialization (i.e., 50%).

Our results point to the possibility that sparsity comes from the training dynamic. Namely, at early training stage with any training data and a random initialization of network parameters, the descending direction

of the gradient on the Transformer parameters tends to point to a regime where their MLPs produce sparse activation maps. In the following, we provide theoretical evidence for this argument by looking at the gradient on the positive activation maps for a DNN with last two layers being a ReLU followed by a fully connected layer. In particular, we have the follow result.

**Theorem 3.1.** *Let  $f(\mathbf{x}; \mathbf{V}, \boldsymbol{\theta}) : \mathbb{R}^n \rightarrow \mathbb{R}^K$  be a neural network given by*

$$f(\mathbf{x}) = \mathbf{V}\sigma(\mathbf{p}(\mathbf{x}; \boldsymbol{\theta})), \quad (3)$$

where  $\mathbf{V} = [\mathbf{v}_1, \dots, \mathbf{v}_{d_f}] \in \mathbb{R}^{K \times d_f}$  is network parameter for the last layer drawn from a random distribution,  $\sigma()$  is the ReLU activation function, and  $\mathbf{p}(\mathbf{x}; \boldsymbol{\theta})$  denotes all other layers with parameter  $\boldsymbol{\theta}$ . We write  $\mathbf{p} = \mathbf{p}(\mathbf{x}; \boldsymbol{\theta})$  for simplicity.

- Consider the mean squared error (MSE) loss  $\ell_{\text{MSE}}(f(\mathbf{x}), \mathbf{y}) \doteq \frac{1}{2} \|f(\mathbf{x}) - \mathbf{y}\|_2^2$ , where  $\mathbf{y}$  is an arbitrary vector independent of  $\mathbf{V}$ . Assume that  $\mathbf{V}$  satisfies

$$\mathbb{E}[\mathbf{V}] = \mathbf{0}, \text{ and } \mathbb{E}[\langle \mathbf{v}_i, \mathbf{v}_j \rangle] \begin{cases} = 0, & \text{if } i \neq j, \\ > 0, & \text{otherwise}^5. \end{cases} \quad (4)$$

If there exist an  $i^*$  such that  $p_{i^*} > 0$ , then we have

$$\mathbb{E} \left[ \frac{\partial \ell_{\text{MSE}}(f(\mathbf{x}), \mathbf{y})}{\partial p_{i^*}} \right] > 0, \quad (5)$$

where the expectation is taken with respect to randomness in  $\mathbf{V}$ .

- Consider the cross-entropy (CE) loss  $\ell_{\text{CE}}(f(\mathbf{x}), \mathbf{y}) = -\langle \mathbf{y}, \log \frac{\exp(f(\mathbf{x}))}{\langle \exp(f(\mathbf{x})), \mathbf{1} \rangle} \rangle$ , where  $\mathbf{y}$  is an arbitrary vector that sums up to one and independent of  $\mathbf{V}$ . Assume that the entries of  $\mathbf{V}$  are drawn from independent distributions, the probability of any entry of  $\mathbf{V}$  being 0 is less than 1, and  $\mathbb{E}[\mathbf{V}] = \mathbf{0}$ . If there exist an  $i^*$  such that  $p_{i^*} > 0$ , then we have

$$\mathbb{E} \left[ \frac{\partial \ell_{\text{CE}}(f(\mathbf{x}), \mathbf{y})}{\partial p_{i^*}} \right] > 0, \quad (6)$$

where the expectation is taken with respect to randomness in  $\mathbf{V}$ .

The proof of Theorem 3.1 is provided in Appendix D. Theorem 3.1 states that the gradient of either the MSE or CE loss with respect to any positive activation  $p_{i^*}$  is positive in expectation. Hence, any training algorithm based on negative gradient directions tends to reduce the magnitude of such positive activations, which will lead to a smaller training loss. Here, the expectation is taken with respect to the randomness in the last layer parameter  $\mathbf{V}$ . Hence, our result can be considered as an analysis for DNNs at initialization where weights are often chosen randomly from a fixed distribution. In particular, the required properties for the distribution of  $\mathbf{V}$  in Theorem 3.1 for both MSE and CE losses are satisfied by commonly used initialization methods, such as the one in [18]. On the other hand, Theorem 3.1 does not apply to subsequent training iterations since the label  $\mathbf{y}$  is no longer independent of  $\mathbf{V}$ . However, it can be seen empirically from Figure 1 that the trend of a decreasing percentage of nonzero entries persists for a certain number of iterations during the beginning of training until such a percentage reaches a low level and stays relatively stable until the end of training.

## 4 Efficient, Robust, and Calibrated: Sparsity is All You Need?

Exploiting sparsity is one of the most commonly used strategy for improving the computational efficiency of Transformers. To introduce activation sparsity, previous work has tried using, e.g., an extra controller [19], an extra mixture-of-experts module [20], etc, often with some nontrivial engineering design. The emergence of sparse activation and its prevalence discussed in Section 2 reveals that sparsity actually comes for free without the need of extra engineering for inducing sparsity at all.

In Section 4.1 we discuss how the free sparsity in Transformers brings us free computation efficiency in terms of FLOPs count. In Section 4.2 we introduce Top- $k$  Transformers, a simple modification of Transformers

<sup>5</sup>This requirement is generally satisfied unless the probability of  $\mathbf{v}_i = \mathbf{0}$  is 1.

where a top- $k$  thresholding operation is applied to the activation maps in all MLPs. Top- $k$  Transformer allows us to obtain sparsity for all input to MLPs and throughout training, hence enables the benefit of sparsity to be realized during training and for all data. Finally, in Section 4.3 we show that enforcing sparser activation with smaller values of  $k$  in Top- $k$  Transformer (without any other hacks, tweaks and hyperparameter tuning) bestows Transformers several desired properties, namely, robustness of training with erroneous annotations, less sensitivity to input noise/perturbation, and better confidence calibration of the predictions.

## 4.1 Efficiency for Free

Given an embedding dimension  $d_{\text{model}}$  and an MLP intermediate dimension  $d_{\text{ff}}$ , the computational complexity of a Transformer for an input sequence of length  $N$  is  $\mathcal{O}(Nd_{\text{model}}^2 + N^2d_{\text{model}} + Nd_{\text{model}}d_{\text{ff}})$ , where the first term comes from computing the key, query, and value matrices, the second term comes from computing the self-attention matrix, and the third term comes from the MLP. For a fixed sequence length  $N$ , and considering the fact that  $d_{\text{ff}}$  is often much larger than  $d_{\text{model}}$ , it is arguable that MLP poses the computational bottleneck in large Transformers. In the following, we explain how sparsity in activation map of MLP can be leveraged to significantly reduce its computational cost, without affecting the model performance.

**Efficiency for the Second MLP Layer.** The sparse activation immediately suggests that a lot of the computation for inference with Transformers is not needed at all. That is, while doing dense matrix-matrix multiplications, much of it is about multiplying a vector by a value of zero, which can be avoided to save computation.

Specifically, we consider the second layer of the MLP in (1) which performs the computation

$$\mathbf{V}\mathbf{a}, \quad (7)$$

where  $\mathbf{a} \in \mathbb{R}^{d_{\text{ff}}}$  is the intermediate activation map of MLP (see (2)) and  $\mathbf{V} \in \mathbb{R}^{d_{\text{model}} \times d_{\text{ff}}}$  is the layer parameter. Eq. (7) involves a simple matrix-vector multiplication which has a FLOP count of  $2d_{\text{model}} \times d_{\text{ff}}$ . However, if  $\mathbf{a}$  is sparse with, say  $s$  nonzero entries, then the FLOP count for (7) reduces to  $2d_{\text{model}} \times s$ . Hence,

$$\text{FLOP in the second MLP layer is reduced by a factor of } 1 - \frac{s}{d_{\text{ff}}}.$$

Note that  $\frac{s}{d_{\text{ff}}}$  is exactly the percentage of nonzeros plotted in the y-axis of e.g. Figure 1, which is 2.7% averaged across all layers. Hence, the computational cost of the second MLP layer can be reduced by a significant amount. More excitingly, the reduction factor  $1 - \frac{s}{d_{\text{ff}}}$  is likely to be even bigger for larger Transformer models (see Figures 4a and 4b), pointing to a greater reduction in computation.

**Efficiency for the First MLP Layer.** The sparsity in the intermediate activation map of MLP does not immediately suggest a reduction in computation for the first MLP layer. Nonetheless, it is possible to significantly reduce the computation in the first MLP layer by leveraging approximate nearest neighbor search, which we explain next.

Recall from (1) that the computation in the first MLP layer is given by

$$\sigma(\mathbf{K}^\top \mathbf{x}), \quad (8)$$

with  $\mathbf{K} = [\mathbf{k}_1, \dots, \mathbf{k}_{d_{\text{ff}}}] \in \mathbb{R}^{d_{\text{model}} \times d_{\text{ff}}}$  being the layer parameter and  $\mathbf{x}$  being the layer input. If the output is sparse with  $k$  nonzero entries, then the calculation in (8) may be formulated as finding  $k$  points from the set  $\{\mathbf{k}_i\}_{i=1}^{d_{\text{ff}}}$  that are “closest” to the input  $\mathbf{x}$  measured by values of inner product. Such a problem is well-known as the nearest neighbor search (NNS) problem or the maximum inner product search problem. While naive solving of the NNS problem has linear complexity in  $d_{\text{ff}}$ , there exists *approximate* algorithms [21, 22, 23, 24] that are of sublinear complexity, and using them in Transformers means that

$$\text{FLOP in the first MLP layer may be reduced to have sublinear complexity in } d_{\text{ff}}.$$

There are of course the questions of whether such approximate NNS algorithms hurt Transformer performance or not, which we leave for future study.

Finally, while the gain in efficiency discussed above is measured by FLOPs, the methods therein require computation with *unstructured* sparsity and data-dependent sparsity patterns, which are usually not well supported on computation hardwares such as TPUs and GPUs. As a result, they do not necessarily translate to walltime reductions with naive implementations. In the next section, we present a Top- $k$  Transformer with



Figure 6: Training and evaluation accuracy of Top- $k$  T5 for three different sizes: base, large and 3B (left) and Top- $k$  ViT (right) with varying  $k$ . *Top- $k$  Transformer is on par with regular Transformer for a large enough  $k$ . E.g. for T5 3B with  $k = 128$ , and ViT with  $k = 256$ , the drop is around 0.3%.*

sparse computation realized by the implementation in [24], which we show to bring walltime reduction for certain cases. We leave a study of more general implementation of sparse computation for obtaining walltime reduction to future work.

## 4.2 Controlling Sparsity with Top- $k$ Transformers

The benefits in terms of efficiency discussed in Section 4.1 comes with caveats. First, while the activation maps are sparse on average, there is the possibility that some of the activation maps for certain inputs are denser hence cannot benefit from sparse computation. Second, sparsity occurs only in trained Transformers while the computation is dense during and particularly at the beginning of training.

Here we present Top- $k$  Transformer, a simple modification to Transformer architecture that allows us to control sparsity level for all model inputs, and throughout training. Top- $k$  Transformer is built upon a regular Transformer with the only modification being the MLP layers, where at the output of the activation function  $\sigma()$  (see (1)) we add a Top- $k$  thresholding operator. That is, the MLPs of Top- $k$  Transformers perform the following computation

$$f(\mathbf{x}; \mathbf{K}, \mathbf{V}) = \mathbf{V} \cdot \text{Top}_k(\sigma(\mathbf{K}^T \mathbf{x})), \quad (9)$$

where  $\text{Top}_k(\cdot)$  performs a thresholding that all entries other than those of the largest  $k$  values are set to zero with  $k$  being a hyper-parameter subject to design choices. Note that Top- $k$  Transformer reduces to a regular Transformer if we set  $k = d_{\text{ff}}$ . By using a small value of  $k$ , the benefit of efficiency in terms of reduction in FLOP as discussed in Section 4.1 applies to Transformer training as well.

The immediate question for Top- $k$  Transformer is whether it offers controllable sparsity at the cost of a reduced performance. Here we conduct experiments with Top- $k$  T5 and Top- $k$  ViT, and evaluate their performance measured by prediction accuracy for C4 span corruption and ImageNet-21k classification tasks, respectively. The results are provided in Figure 6. We see that with the Top- $k$  T5 (resp., Top- $k$  ViT) Transformer, taking  $k$  to be 64 (resp., 256) is sufficient for closely matching the test performance of the vanilla T5 (resp., ViT). Note that this is achieved without any other hyper-parameter tuning for the Top- $k$  Transformers upon those used for a regular Transformer, and it is possible that other hyper-parameter choices may further improve the performance of Top- $k$  Transformers.

Finally, we evaluate the benefit of Top- $k$  in terms of reducing inference latency. In our experiment, we add a Top- $k$  thresholding to T5X [25] with the implementation of `jax.lax.approx_max_k` [24] using a recall target of 0.95. Then, we evaluate the decoder per-token wall time for unbatched greedy decoding during inference on a single TPUv4 chip. The results with varying model sizes and varying values of  $k$  are

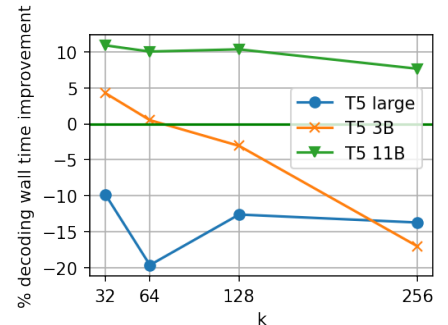


Figure 7: Latency reduction for unbatched greedy decoding in decoder of Top- $k$  Transformers on TPUv4.

Table 1: Evaluation of Top-128 ViT for ImageNet-1k classification in terms of 1) natural accuracy with ImageNet-1k evaluation set, 2) robust accuracy with  $\{40\%, 80\%\}$  corrupted training labels, 3) robust accuracy under input perturbation with additive  $\{\text{Gaussian, Impulse, Shot}\}$  noise on evaluation images, and 4) calibration error on evaluation data measured by ECE. *Top-128 ViT is on par with ViT for natural accuracy while is significantly better for model robustness and calibration.*

Methods	Natural Accuracy	Accuracy w/ Train Label Noise		Accuracy under Input Perturbation			Expected Calibration Error (ECE)
		40%	80%	Gaussian	Impulse	Shot	
ViT	74.85%	59.44%	25.35%	39.54%	37.37%	38.56%	8.42%
Top-128 ViT	74.83%	62.13%	30.80%	42.29%	40.07%	40.68%	7.48%

presented in Figure 7. We observe that larger models have more wall time reduction, due to the fact that they have larger  $d_{\text{ff}}$  hence more FLOPs reduction by our discussion in Section 4.1. In particular, for T5-11B we observe around 10% wall time reduction with  $k \leq 128$ , though this amount becomes smaller with a larger  $k = 256$ .

### 4.3 Bonus! Improved Robustness and Calibration

Despite not being explicitly designed for such purposes, inducing sparse activation via Top- $k$  Transformer has the benefits of improving model robustness<sup>6</sup> and confidence calibration. We demonstrate this using the image classification task with the ImageNet-1k dataset, and present a snapshot of key results in Table 1. All results for Top- $k$  ViT are obtained without any model and training hyper-parameter tuning upon those for ViT. Contexts, details, and full results are presented below.

**Robustness to Label Noise.** An important challenge for DNNs is that they are highly susceptible to label noise, the problem where a certain percentage of training labels are corrupted or erroneously generated. This may be attributed to the fact that DNNs are often over-parameterized, hence too “capable” that they tend to overfit, or “memorize” the noisy labels without generalizing to test data. While many dedicated techniques exist (see e.g., [26, 27] for a review), here we show that a simple Top- $k$  Transformer with a small value of  $k$  can effectively address the label noise issue.

We conduct experiments using the ImageNet-1k dataset for which we replace  $p\%$  of the labels in the training set with a random label drawn uniformly from the set of all possible labels. In Figure 8 we present the training and evaluation accuracy curves for  $p = 80\%$ . It can be seen that the vanilla ViT starts to overfit at around 45,000 steps where the training accuracy continues to increase but the evaluation accuracy starts to drop. In contrast, the evaluation performance of Top-128 ViT continues to improve until the end of training, which leads to a better final performance. The final evaluation performance under  $p \in \{40\%, 80\%\}$  label noise is presented in Table 1. It shows that Top- $k$  offers a consistent performance gain with label noise.

**Confidence Calibration.** Aside from the label noise issue, another symptom of over-parameterization of DNNs is that they tend to be overly confident in their predictions. In the context of classification problems, they tend to assign a high (i.e., close to 1) probability to the class of its prediction, while it is more desirable that they produce a probability that is commensurate with its confidence level [28]. A commonly used metric for confidence calibration is the expected calibration error (ECE) [29], which is the discrepancy between the probability to the class of a model’s prediction and the probability that its prediction is actually correct.

<sup>6</sup>This is previously demonstrated in [11] for ConvNets.

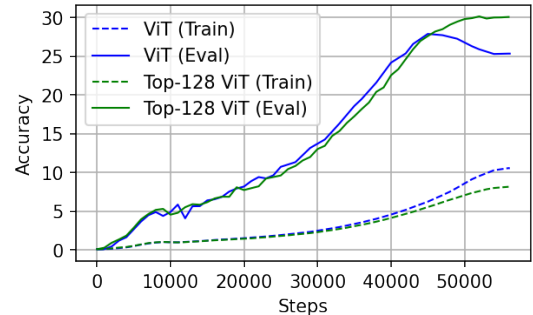


Figure 8: Training curves of Top-128 ViT under 80% label noise for ImageNet-1k classification.

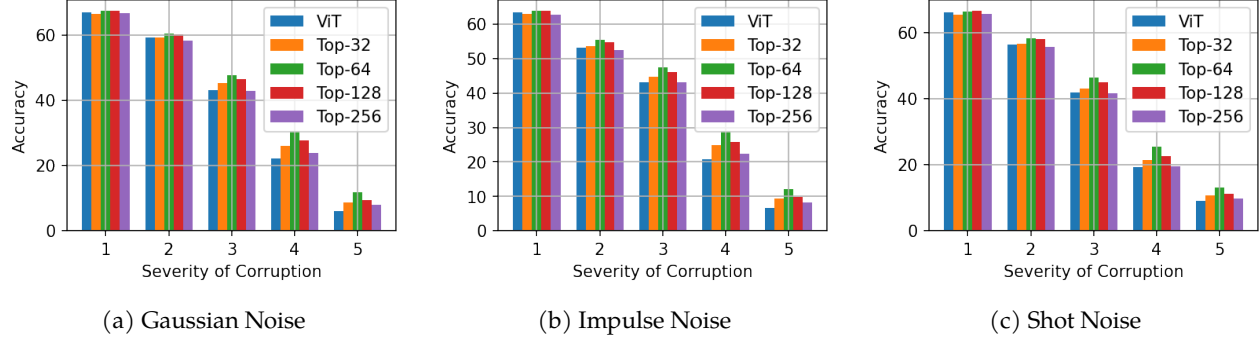


Figure 10: Performance of Top- $k$  ViT on corrupted ImageNet-1k test data with Gaussian noise (left), impulse noise (middle), and shot noise (right), each under five severity levels. Top- $k$  improves robustness for all noise types and on all corruption levels with a suitable choice of  $k$ .

Here we measure the calibration of Top- $k$  ViT via ECE and report the results in Figure 9. At the beginning of training the model has a low ECE because the output probabilities are mostly uniformly distributed across all classes hence the model is not confident, and that its prediction is purely random hence wrong with high probability. The model tends to become overly confident as the training progresses, hence the ECE increases particularly towards the end of training. What we can observe is that Top- $k$  enables the Transformer to be more calibrated when compared to a vanilla Transformer, particularly for small values of  $k$ . The results with  $k = 128$  and its comparison with the vanilla ViT is also presented in Table 1.

**Robustness to Input Perturbation.** Another important challenge with DNNs is that their outputs tend to be sensitive to naturally occurring image corruptions, which limits their application to mission critical tasks [30]. Here we evaluate the robustness of Top- $k$  ViT to three types of additive noises, namely Gaussian noise, impulse noise, and shot noise. For that purpose, we train Top- $k$  ViT on standard ImageNet-1k training data and report their classification accuracy on ImageNet-C [31], a benchmark that contains algorithmically generated Gaussian, impulse, and shot noise (among many others types) applied to the ImageNet-1k test dataset. For each noise type, there are five severity levels for which the results are all presented in Figure 10. We can see that Top- $k$  ViT offers a performance gain over the vanilla ViT, particular with  $k = 64$  or  $k = 128$  and the severity level is high. We also report the averaged performance over all severity levels of each corruption type in Table 1.

## 5 Related Work

Prior efforts on introducing sparsity in deep neural networks abound, though often with diverse motivations and objectives. Here we provide a brief overview of several popular lines of work.

**Sparsity for Efficiency.** Due to the high computational cost of dense matrix operations in standard DNNs, a plethora of work has explored sparsity in either model weights or activation maps for improving training and inference efficiency (see e.g. [10] for a review). For activation sparsity in particular, sparsity for efficiency is explored perhaps first in convolutional neural networks [32, 33, 34] before subsequently becomes a key design component in many of the largest Transformer based language and vision models [20, 35, 36, 37]. The Top- $k$  thresholding that we use in Top- $k$  Transformer has also been previously used in [12] to improve memory efficiency of Transformers. However, it has been unclear *a priori* whether sparsity hurts model performance, hence the practice often relies on wishful design, trial-and-error, and post-hoc justification [38]. Our discovery that Transformers naturally produce sparse activation maps, and that larger models are even sparser, may

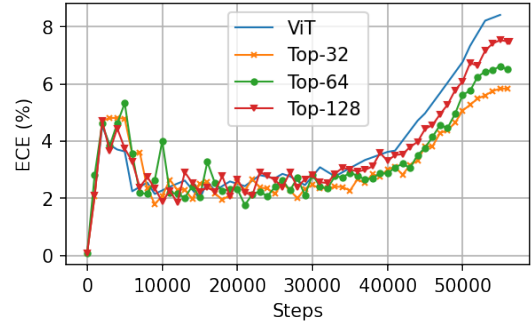


Figure 9: Confidence calibration of Top- $k$  ViT for ImageNet-1k classification.

provide principled perspectives towards efficiently training future large models.

**Sparsity for Robustness.** Many work find that smaller networks obtained by model compression are more robust to adversarial perturbation [39, 40, 41] and label noise [42]. Another line of work that uses sparsity for robustness leverages the property that practical data corruption is often sparse [43, 44, 45]. None of the work mentioned above is based on sparsity in activation maps. More closely related to ours is the work [11] where sparsity in activation map of convolutional DNNs is shown to improve robustness to input perturbation, and the work [46] that leverages sparse activation to derive robust generalization error bounds.

**Sparsity for Explainability.** Work on leveraging sparsity for interpreting deep learning models long exist but often in a post-hoc fashion for examining the semantic meanings encoded by a neuron of a trained model [47]. For Transformers, evidence suggests that the learned knowledge is encoded mainly in its MLPs with individual neurons expressing specific factual knowledge [48]. Moreover, enforcing neuron activation sparsity in MLPs helps to improve the percentage of neurons that are interpretable [49]. Hence, our discovery may point to new directions towards developing more interpretable DNNs [50, 51].

**Sparsity for Data Modeling.** Following the seminal work [8] on the emergence of V1 receptive fields in primary visual cortex from sparse encoding of natural images, there are a lot of interests in sparsity as an effective modeling of natural signals [52]. With the popularity of deep learning techniques and the close resemblance of the computational structure of ReLU networks and sparse encoding algorithms [53], it became natural to study a DNN as a multi-layer sparse modeling of the data [54]. Along with substantial theoretical understanding of such a modeling are obtained [55, 56], there are also experimental results on their practical benefits [57] though less often on modern large-scale data. Our discovery on the sparsity of Transformers offers evidence in favor of the perspective that deep neural networks perform sparse modeling of data, and may motivate the design of more practical sparse modeling in the future.

**Sparsity for Theory of Over-parameterized Models.** Because of its simplicity and well-developed theory in classical machine learning [58, 15, 16], sparse modeling is often used to provide theoretical understanding of modern large and over-parameterized models. This include works on implicit regularization [59, 60, 61, 62, 63], nonconvex optimization [64, 65], noise interpolators [66, 67, 68], etc. However, the aforementioned work uses sparsity as a testbed or toy model to gain insights, without implication of existence of sparsity in DNNs.

## 6 Discussion: Transformers are Parsimonious Models?

As the scale of deep learning models continues to grow, it may have been taken for granted that increasing model size is necessary and possibly even sufficient for obtaining ever-improving performance. However, historically the futuristic picture for large scale DNNs had not been entirely optimistic. For example, Geman et al. in 1992 [69] made an argument based on the notion of bias-variance trade-off that despite their excellent goodness-of-fit to training data, DNNs may suffer from a high prediction variance hence poor generalization performance. While recent evidence suggests that DNNs exhibit an unexpected unimodal shaped variance curve [70] where variance is controlled in the over-parameterized regime by an implicit algorithmic regularization, it is largely unclear whether such a regularization is pertinent and accounts for the good generalization of practical DNNs.

The emergence of sparse activation in Transformer models discussed in Section 2 (see also Appendix B) may offer an explanation for why DNNs work well and do not overfit. The notion of sparsity pertains to the law of parsimony, a.k.a. *Occam’s razor*, where among all possible explanations of observed data, the *simplest* ones are preferred. As a fundamental scientific principle, the law of parsimony is broadly used in various scientific and engineering subjects [71, 72], including classical machine learning [73]. However, it is often not a critical design component in DNNs and goes against the recent deep learning practice of training increasingly flexible, redundant, and powerful models. Hence, our discovery may be rather surprising. Even not explicitly designed so, Transformers only use a small fraction of its parameters to parse a given input, hence may be regarded as parsimonious models as well. As discussed in Section 3.4, sparsity may arise from the dynamic of neural network training rather than any explicit sparsity regularizer. More importantly, evidence of improved robustness and calibration in Section 4.3 indicates that sparsity is a pertinent prior for its good generalization.

**Outlook.** The emergence of sparsity and its many practical benefits point to sparsity and the law of parsimony

as a fundamental component of more powerful models in the future<sup>7</sup>. Along that line, our work is merely a starting point and may have brought more challenges than it has solved. While enforcing sparsity via Top- $k$  thresholding demonstrates benefits, it is used as a proof-of-concept due to its simplicity and is not meant to be the best way of inducing sparsity. The hope is that our results may motivate future study of introducing sparsity in DNNs in a more principled way. Moreover, while sparsity readily implies a drastically reduced computational cost in terms of FLOP count, the benefit may not be reflected by wall time since existing deep learning platforms are often geared towards efficient dense computation. Hence, our result may motivate the design of future platforms that excel at sparse computation. Finally, while our motivation of studying sparse activation in Transformers comes (partly) from study of biological brains, establishing such a connection may reciprocally benefit efforts on applying artificial intelligence to the study of biology and neuroscience [79].

## Acknowledgments

We would like to acknowledge helpful discussions with René Vidal and Jeremias Sulam from Johns Hopkins University, with Weijie Su from UPenn, with Yuxiang Wang from UC Santa Barbara, with Atlas Wang from UT Austin, with Nishanth Dikkala, Nikhil Vyas, Preston McAfee and Mukund Sundararajan from Google, with Subutai Ahmad from Numenta, with Wei Hu, Salar Fattah, and Jianhao Ma from University of Michigan, with Tuo Zhao from Georgia Tech. We particularly thank Donhauser Konstantin from ETH Zurich for interesting discussion on hypothesis for emergence of sparsity.

## References

- [1] Yann LeCun, Yoshua Bengio, and Geoffrey Hinton. Deep learning. *nature*, 521(7553):436–444, 2015.
- [2] Jason ND Kerr, David Greenberg, and Fritjof Helmchen. Imaging input and output of neocortical networks in vivo. *Proceedings of the National Academy of Sciences*, 102(39):14063–14068, 2005.
- [3] Cindy Poo and Jeffry S Isaacson. Odor representations in olfactory cortex: “sparse” coding, global inhibition, and oscillations. *Neuron*, 62(6):850–861, 2009.
- [4] Alison L Barth and James FA Poulet. Experimental evidence for sparse firing in the neocortex. *Trends in neurosciences*, 35(6):345–355, 2012.
- [5] Mohsin S Ahmed, James B Priestley, Angel Castro, Fabio Stefanini, Ana Sofia Solis Canales, Elizabeth M Balough, Erin Lavoie, Luca Mazzucato, Stefano Fusi, and Attila Losonczy. Hippocampal network reorganization underlies the formation of a temporal association memory. *Neuron*, 107(2):283–291, 2020.
- [6] Ashish Vaswani, Noam Shazeer, Niki Parmar, Jakob Uszkoreit, Llion Jones, Aidan N Gomez, Łukasz Kaiser, and Illia Polosukhin. Attention is all you need. *Advances in neural information processing systems*, 30, 2017.
- [7] Colin Raffel, Noam Shazeer, Adam Roberts, Katherine Lee, Sharan Narang, Michael Matena, Yanqi Zhou, Wei Li, Peter J Liu, et al. Exploring the limits of transfer learning with a unified text-to-text transformer. *J. Mach. Learn. Res.*, 21(140):1–67, 2020.
- [8] Bruno A Olshausen and David J Field. Emergence of simple-cell receptive field properties by learning a sparse code for natural images. *Nature*, 381(6583):607–609, 1996.
- [9] Zhengyan Zhang, Yankai Lin, Zhiyuan Liu, Peng Li, Maosong Sun, and Jie Zhou. Moefication: Transformer feed-forward layers are mixtures of experts. In *Findings of the Association for Computational Linguistics: ACL 2022*, pages 877–890, 2022.
- [10] Torsten Hoefler, Dan Alistarh, Tal Ben-Nun, Nikoli Dryden, and Alexandra Peste. Sparsity in deep learning: Pruning and growth for efficient inference and training in neural networks. *J. Mach. Learn. Res.*, 22(241):1–124, 2021.
- [11] Subutai Ahmad and Luiz Scheinkman. How can we be so dense? the benefits of using highly sparse representations. *arXiv preprint arXiv:1903.11257*, 2019.

---

<sup>7</sup>This view resonates with recent work on the pathway to artificial intelligence [74, 75, 76, 77, 78].

[12] Ankit Gupta, Guy Dar, Shaya Goodman, David Ciprut, and Jonathan Berant. Memory-efficient transformers via top-k attention. In *Proceedings of the Second Workshop on Simple and Efficient Natural Language Processing*, pages 39–52, 2021.

[13] Alexey Dosovitskiy, Lucas Beyer, Alexander Kolesnikov, Dirk Weissenborn, Xiaohua Zhai, Thomas Unterthiner, Mostafa Dehghani, Matthias Minderer, Georg Heigold, Sylvain Gelly, Jakob Uszkoreit, and Neil Houlsby. An image is worth 16x16 words: Transformers for image recognition at scale. In *International Conference on Learning Representations*, 2021.

[14] Jia Deng, Wei Dong, Richard Socher, Li-Jia Li, Kai Li, and Li Fei-Fei. Imagenet: A large-scale hierarchical image database. In *2009 IEEE conference on computer vision and pattern recognition*, pages 248–255. Ieee, 2009.

[15] Rene Vidal, Yi Ma, and Shankar Sastry. Generalized principal component analysis. *Interdisciplinary Applied Mathematics*, 43:22–23, 2015.

[16] John Wright and Yi Ma. *High-Dimensional Data Analysis with Low-Dimensional Models: Principles, Computation, and Applications*. Cambridge University Press, 2022.

[17] Chiyuan Zhang, Samy Bengio, Moritz Hardt, Benjamin Recht, and Oriol Vinyals. Understanding deep learning (still) requires rethinking generalization. *Communications of the ACM*, 64(3):107–115, 2021.

[18] Kaiming He, Xiangyu Zhang, Shaoqing Ren, and Jian Sun. Delving deep into rectifiers: Surpassing human-level performance on imagenet classification. In *Proceedings of the IEEE international conference on computer vision*, pages 1026–1034, 2015.

[19] Sebastian Jaszczur, Aakanksha Chowdhery, Afroz Mohiuddin, Lukasz Kaiser, Wojciech Gajewski, Henryk Michalewski, and Jonni Kanerva. Sparse is enough in scaling transformers. *Advances in Neural Information Processing Systems*, 34:9895–9907, 2021.

[20] William Fedus, Barret Zoph, and Noam Shazeer. Switch transformers: Scaling to trillion parameter models with simple and efficient sparsity. *Journal of Machine Learning Research*, 23(120):1–39, 2022.

[21] Anshumali Shrivastava and Ping Li. Asymmetric lsh (alsh) for sublinear time maximum inner product search (mips). *Advances in neural information processing systems*, 27, 2014.

[22] Jeff Johnson, Matthijs Douze, and Hervé Jégou. Billion-scale similarity search with GPUs. *IEEE Transactions on Big Data*, 7(3):535–547, 2019.

[23] Ruiqi Guo, Philip Sun, Erik Lindgren, Quan Geng, David Simcha, Felix Chern, and Sanjiv Kumar. Accelerating large-scale inference with anisotropic vector quantization. In *International Conference on Machine Learning*, pages 3887–3896. PMLR, 2020.

[24] Felix Chern, Blake Hechtman, Andy Davis, Ruiqi Guo, David Majnemer, and Sanjiv Kumar. Tpu-knn: K nearest neighbor search at peak flop/s. *arXiv preprint arXiv:2206.14286*, 2022.

[25] Adam Roberts, Hyung Won Chung, Anselm Levskaya, Gaurav Mishra, James Bradbury, Daniel Andor, Sharan Narang, Brian Lester, Colin Gaffney, Afroz Mohiuddin, Curtis Hawthorne, Aitor Lewkowycz, Alex Salcianu, Marc van Zee, Jacob Austin, Sebastian Goodman, Livio Baldini Soares, Haitang Hu, Sasha Tsvyashchenko, Aakanksha Chowdhery, Jasmijn Bastings, Jannis Bulian, Xavier Garcia, Jianmo Ni, Andrew Chen, Kathleen Kenealy, Jonathan H. Clark, Stephan Lee, Dan Garrette, James Lee-Thorp, Colin Raffel, Noam Shazeer, Marvin Ritter, Maarten Bosma, Alexandre Passos, Jeremy Maitin-Shepard, Noah Fiedel, Mark Omernick, Brennan Saeta, Ryan Sepassi, Alexander Spiridonov, Joshua Newlan, and Andrea Gesmundo. Scaling up models and data with t5x and seqio. *arXiv preprint arXiv:2203.17189*, 2022.

[26] Görkem Algan and Ilkay Ulusoy. Image classification with deep learning in the presence of noisy labels: A survey. *Knowledge-Based Systems*, 215:106771, 2021.

[27] Hwanjun Song, Minseok Kim, Dongmin Park, Yooju Shin, and Jae-Gil Lee. Learning from noisy labels with deep neural networks: A survey. *IEEE Transactions on Neural Networks and Learning Systems*, 2022.

[28] Chuan Guo, Geoff Pleiss, Yu Sun, and Kilian Q Weinberger. On calibration of modern neural networks. In *International conference on machine learning*, pages 1321–1330. PMLR, 2017.

[29] Mahdi Pakdaman Naeini, Gregory Cooper, and Milos Hauskrecht. Obtaining well calibrated probabilities using bayesian binning. In *Twenty-Ninth AAAI Conference on Artificial Intelligence*, 2015.

[30] Srinadh Bhojanapalli, Ayan Chakrabarti, Daniel Glasner, Daliang Li, Thomas Unterthiner, and Andreas Veit. Understanding robustness of transformers for image classification. In *Proceedings of the IEEE/CVF International Conference on Computer Vision*, pages 10231–10241, 2021.

[31] Dan Hendrycks and Thomas Dietterich. Benchmarking neural network robustness to common corruptions and perturbations. In *International Conference on Learning Representations*, 2019.

[32] Minsoo Rhu, Mike O’Connor, Niladri Chatterjee, Jeff Pool, Youngeun Kwon, and Stephen W Keckler. Compressing dna engine: Leveraging activation sparsity for training deep neural networks. In *2018 IEEE International Symposium on High Performance Computer Architecture (HPCA)*, pages 78–91. IEEE, 2018.

[33] Georgios Georgiadis. Accelerating convolutional neural networks via activation map compression. In *Proceedings of the IEEE/CVF Conference on Computer Vision and Pattern Recognition*, pages 7085–7095, 2019.

[34] Mark Kurtz, Justin Kopinsky, Rati Gelashvili, Alexander Matveev, John Carr, Michael Goin, William Leiserson, Sage Moore, Nir Shavit, and Dan Alistarh. Inducing and exploiting activation sparsity for fast inference on deep neural networks. In *International Conference on Machine Learning*, pages 5533–5543. PMLR, 2020.

[35] Nan Du, Yanping Huang, Andrew M Dai, Simon Tong, Dmitry Lepikhin, Yuanzhong Xu, Maxim Krikun, Yanqi Zhou, Adams Wei Yu, Orhan Firat, et al. Glam: Efficient scaling of language models with mixture-of-experts. In *International Conference on Machine Learning*, pages 5547–5569. PMLR, 2022.

[36] Samyam Rajbhandari, Conglong Li, Zhewei Yao, Minjia Zhang, Reza Yazdani Aminabadi, Ammar Ahmad Awan, Jeff Rasley, and Yuxiong He. Deepspeed-moe: Advancing mixture-of-experts inference and training to power next-generation ai scale. *arXiv preprint arXiv:2201.05596*, 2022.

[37] William Fedus, Jeff Dean, and Barret Zoph. A review of sparse expert models in deep learning. *arXiv preprint arXiv:2209.01667*, 2022.

[38] Cenk Baykal, Nishanth Dikkala, Rina Panigrahy, Cyrus Rashtchian, and Xin Wang. A theoretical view on sparsely activated networks. *arXiv preprint arXiv:2208.04461*, 2022.

[39] Yiwen Guo, Chao Zhang, Changshui Zhang, and Yurong Chen. Sparse dnns with improved adversarial robustness. *Advances in neural information processing systems*, 31, 2018.

[40] Artur Jordao and Hélio Pedrini. On the effect of pruning on adversarial robustness. In *Proceedings of the IEEE/CVF International Conference on Computer Vision*, pages 1–11, 2021.

[41] Tianlong Chen, Zhenyu Zhang, Santosh Balachandra, Haoyu Ma, Zehao Wang, Zhangyang Wang, et al. Sparsity winning twice: Better robust generalization from more efficient training. In *International Conference on Learning Representations*, 2022.

[42] Yihao Xue, Kyle Whitecross, and Baharan Mirzasoleiman. Superior generalization of smaller models in the presence of significant label noise. *arXiv preprint arXiv:2208.08003*, 2022.

[43] Aritra Ghosh, Himanshu Kumar, and PS Sastry. Robust loss functions under label noise for deep neural networks. In *Proceedings of the Thirty-First AAAI Conference on Artificial Intelligence*, pages 1919–1925, 2017.

[44] Chong You, Zhihui Zhu, Qing Qu, and Yi Ma. Robust recovery via implicit bias of discrepant learning rates for double over-parameterization. *Advances in Neural Information Processing Systems*, 33:17733–17744, 2020.

[45] Sheng Liu, Zhihui Zhu, Qing Qu, and Chong You. Robust training under label noise by over-parameterization. In *International Conference on Machine Learning*, 2022.

[46] Ramchandran Muthukumar and Jeremias Sulam. Adversarial robustness of sparse local lipschitz predictors. *arXiv preprint arXiv:2202.13216*, 2022.

[47] Fahim Dalvi, Nadir Durrani, Hassan Sajjad, Yonatan Belinkov, Anthony Bau, and James Glass. What is one grain of sand in the desert? analyzing individual neurons in deep nlp models. In *Proceedings of the AAAI Conference on Artificial Intelligence*, pages 6309–6317, 2019.

[48] Damai Dai, Li Dong, Yaru Hao, Zhifang Sui, Baobao Chang, and Furu Wei. Knowledge neurons in pretrained transformers. In *Proceedings of the 60th Annual Meeting of the Association for Computational Linguistics (Volume 1: Long Papers)*, pages 8493–8502, 2022.

[49] Nelson Elhage, Tristan Hume, Catherine Olsson, Neel Nanda, Tom Henighan, Scott Johnston, Sheer ElShowk, Nicholas Joseph, Nova DasSarma, Ben Mann, Danny Hernandez, Amanda Askell, Kamal Ndousse, Jones, , Dawn Drain, Anna Chen, Yuntao Bai, Deep Ganguli, Liane Lovitt, Zac Hatfield-Dodds, Jackson Kernion, Tom Conerly, Shauna Kravec, Stanislav Fort, Saurav Kadavath, Josh Jacobson, Eli Tran-Johnson, Jared Kaplan, Jack Clark, Tom Brown, Sam McCandlish, Dario Amodei, and Christopher Olah. Softmax linear units. *Transformer Circuits Thread*, 2022. <https://transformer-circuits.pub/2022/solu/index.html>.

[50] Xavier Suau Cuadros, Luca Zappella, and Nicholas Apostoloff. Self-conditioning pre-trained language models. In *International Conference on Machine Learning*, pages 4455–4473. PMLR, 2022.

[51] Hassan Sajjad, Nadir Durrani, and Fahim Dalvi. Neuron-level interpretation of deep nlp models: A survey. *arXiv preprint arXiv:2108.13138*, 2021.

[52] Julien Mairal, Francis Bach, Jean Ponce, et al. Sparse modeling for image and vision processing. *Foundations and Trends® in Computer Graphics and Vision*, 8(2-3):85–283, 2014.

[53] Karol Gregor and Yann LeCun. Learning fast approximations of sparse coding. In *Proceedings of the 27th international conference on international conference on machine learning*, pages 399–406, 2010.

[54] Vardan Petyan, Yaniv Romano, Jeremias Sulam, and Michael Elad. Theoretical foundations of deep learning via sparse representations: A multilayer sparse model and its connection to convolutional neural networks. *IEEE Signal Processing Magazine*, 35(4):72–89, 2018.

[55] Vardan Petyan, Yaniv Romano, and Michael Elad. Convolutional neural networks analyzed via convolutional sparse coding. *The Journal of Machine Learning Research*, 18(1):2887–2938, 2017.

[56] Jeremias Sulam, Vardan Petyan, Yaniv Romano, and Michael Elad. Multilayer convolutional sparse modeling: Pursuit and dictionary learning. *IEEE Transactions on Signal Processing*, 66(15):4090–4104, 2018.

[57] Xiaoxia Sun, Nasser M Nasrabadi, and Trac D Tran. Supervised deep sparse coding networks. In *2018 25th IEEE International Conference on Image Processing (ICIP)*, pages 346–350. IEEE, 2018.

[58] Emmanuel J Candès and Michael B Wakin. An introduction to compressive sampling. *IEEE signal processing magazine*, 25(2):21–30, 2008.

[59] Tomas Vaskevicius, Varun Kanade, and Patrick Rebeschini. Implicit regularization for optimal sparse recovery. *Advances in Neural Information Processing Systems*, 32, 2019.

[60] Peng Zhao, Yun Yang, and Qiao-Chu He. Implicit regularization via hadamard product over-parametrization in high-dimensional linear regression. *arXiv preprint arXiv:1903.09367*, 2019.

[61] Blake Woodworth, Suriya Gunasekar, Jason D Lee, Edward Moroshko, Pedro Savarese, Itay Golan, Daniel Soudry, and Nathan Srebro. Kernel and rich regimes in overparametrized models. In *Conference on Learning Theory*, pages 3635–3673. PMLR, 2020.

[62] Hung-Hsu Chou, Johannes Maly, and Holger Rauhut. More is less: Inducing sparsity via overparameterization. *arXiv preprint arXiv:2112.11027*, 2021.

[63] Mor Shpigel Nacson, Kavya Ravichandran, Nathan Srebro, and Daniel Soudry. Implicit bias of the step size in linear diagonal neural networks. In *International Conference on Machine Learning*, pages 16270–16295. PMLR, 2022.

[64] Rares-Darius Buhai, Yoni Halpern, Yoon Kim, Andrej Risteski, and David Sontag. Empirical study of the benefits of overparameterization in learning latent variable models. In *International Conference on Machine Learning*, pages 1211–1219. PMLR, 2020.

[65] Jeremias Sulam, Chong You, and Zhihui Zhu. Recovery and generalization in over-realized dictionary learning. *Journal of Machine Learning Research*, 23(135):1–23, 2022.

[66] Geoffrey Chinot, Matthias Löffler, and Sara van de Geer. On the robustness of minimum norm interpolators and regularized empirical risk minimizers. *The Annals of Statistics*, 50(4):2306–2333, 2022.

[67] Frederic Koehler, Lijia Zhou, Danica J Sutherland, and Nathan Srebro. Uniform convergence of interpolators: Gaussian width, norm bounds and benign overfitting. In *Advances in Neural Information Processing Systems*, 2021.

[68] Konstantin Donhauser, Nicolo Ruggeri, Stefan Stojanovic, and Fanny Yang. Fast rates for noisy interpolation require rethinking the effects of inductive bias. *arXiv preprint arXiv:2203.03597*, 2022.

[69] Stuart Geman, Elie Bienenstock, and René Doursat. Neural networks and the bias/variance dilemma. *Neural computation*, 4(1):1–58, 1992.

[70] Zitong Yang, Yaodong Yu, Chong You, Jacob Steinhardt, and Yi Ma. Rethinking bias-variance trade-off for generalization of neural networks. In *International Conference on Machine Learning*, pages 10767–10777. PMLR, 2020.

[71] Robert Epstein. The principle of parsimony and some applications in psychology. *The Journal of Mind and Behavior*, pages 119–130, 1984.

[72] Pedro Domingos. The role of occam’s razor in knowledge discovery. *Data mining and knowledge discovery*, 3(4):409–425, 1999.

[73] Robert Tibshirani. Regression shrinkage and selection via the lasso. *Journal of the Royal Statistical Society: Series B (Methodological)*, 58(1):267–288, 1996.

[74] Paul Barham, Aakanksha Chowdhery, Jeff Dean, Sanjay Ghemawat, Steven Hand, Daniel Hurt, Michael Isard, Hyeontaek Lim, Ruoming Pang, Sudip Roy, et al. Pathways: Asynchronous distributed dataflow for ml. *Proceedings of Machine Learning and Systems*, 4:430–449, 2022.

[75] Daniel A. Roberts. Why is ai hard and physics simple?, 2021.

[76] Yann LeCun. A path towards autonomous machine intelligence. *preprint posted on openreview*, 2022.

[77] Rama K Vasudevan, Maxim Ziatdinov, Lukas Vlcek, and Sergei V Kalinin. Off-the-shelf deep learning is not enough, and requires parsimony, bayesianity, and causality. *npj Computational Materials*, 7(1):1–6, 2021.

[78] Yi Ma, Doris Tsao, and Heung-Yeung Shum. On the principles of parsimony and self-consistency for the emergence of intelligence. *Frontiers of Information Technology & Electronic Engineering*, pages 1–26, 2022.

[79] Blake Richards, Doris Tsao, and Anthony Zador. The application of artificial intelligence to biology and neuroscience. *Cell*, 185(15):2640–2643, 2022.

[80] Diederik P Kingma and Jimmy Ba. Adam: A method for stochastic optimization. In *International Conference on Learning Representations*, 2015.

[81] Jacob Devlin, Ming-Wei Chang, Kenton Lee, and Kristina Toutanova. Bert: Pre-training of deep bidirectional transformers for language understanding. In *Proceedings of NAACL-HLT*, pages 4171–4186, 2019.

[82] Ilya O Tolstikhin, Neil Houlsby, Alexander Kolesnikov, Lucas Beyer, Xiaohua Zhai, Thomas Unterthiner, Jessica Yung, Andreas Steiner, Daniel Keysers, Jakob Uszkoreit, et al. Mlp-mixer: An all-mlp architecture for vision. *Advances in Neural Information Processing Systems*, 34:24261–24272, 2021.

[83] Alex Krizhevsky, Ilya Sutskever, and Geoffrey E Hinton. Imagenet classification with deep convolutional neural networks. *Communications of the ACM*, 60(6):84–90, 2017.

[84] Kaiming He, Xiangyu Zhang, Shaoqing Ren, and Jian Sun. Deep residual learning for image recognition. In *Proceedings of the IEEE conference on computer vision and pattern recognition*, pages 770–778, 2016.

# Appendices

The appendices are organized as follows. In Section A we provide the implementation details for experiments conducted in this paper. In Section B we demonstrate the emergence of sparse activation in other architectures and with other optimizers than those used in Section 2. In Section C we provide additional experiments upon those in Section 4 to demonstrate the benefits of sparsity. In Section D we provide the proof to Theorem 3.1. Finally, in Section E we present insights on the emergence of activation sparsity from experiments on two-layer MLP models.

## A Implementation Details

### A.1 T5

Unless specified otherwise, we use vanilla T5 architecture [7]. We train the models with dropout of 0.1, Adafactor optimizer, and an inverse square root learning rate schedule. For the first 10,000 steps we also use a fixed learning rate of 0.01 as warm-up. The training task is span corruption without any mixture, and unless specified otherwise, we train the model for 100,000 steps with batch size of 256 to save compute and time, as the sparsity or accuracy trend is already clear by then. We use 512 tokens on the encoder side and 114 tokens on the decoder side.

### A.2 ViT

Following [13], we train ViT using ADAM [80] as the optimizer with  $\beta_1 = 0.9, \beta_2 = 0.999$ . Other training details such as weight decay, dropout rate, and learning rate all follow the description in [13, Section B.1] except that we train for 180 epochs (as opposed to 300) on ImageNet-1k.

## B Additional Results On Prevalence of Sparsity

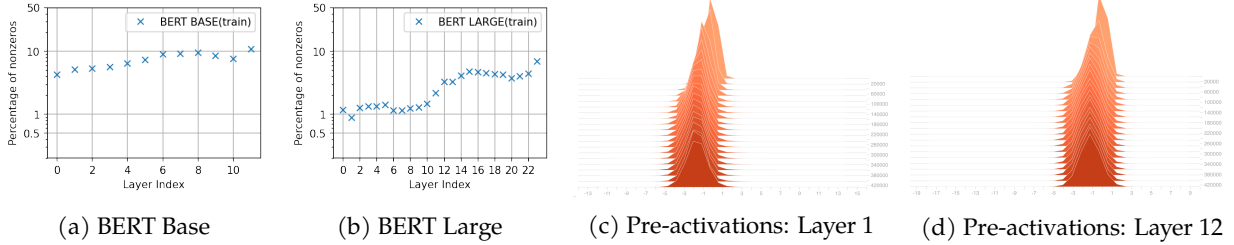


Figure B.1: Plots a, b: Percentage of nonzero entries in activation maps of BERT Base and Large models [81] trained on Wikipedia dataset. We observe high levels of sparsity (<10%) similar to other Transformer models. Plots c, d: Histograms of pre-activation values for layers 1 and 12 of a Bert Base model. We notice that while at initialization the activations are distributed with mean 0, the mean quickly shifts negative as the training progresses, resulting in high levels of sparse activation values.

### B.1 Sparsity and Network Architecture

We evaluate the sparsity level of activation map in several commonly used network architectures beyond T5 and ViT. This includes BERT which is also a Transformer based architecture, as well as non-Transformer based architectures such as MLP-Mixer and ConvNets. We also examine whether residual connection accounts for the emergence of sparsity.

**BERT.** We evaluate the sparsity level of BERT models [81]. We specifically consider BERT Base (12 layers) and BERT Large (24 layers) Transformer models, with ReLU activation in the MLP layers. We follow the same

training recipe as [81] and pre-train these models on Wikipedia and Books dataset using Masked Language Modelling (MLM) objective. We train for 450000 steps with a batch size of 1024 using AdamW optimizer with  $1e - 4$  learning rate.

In Figure B.1 we plot the sparsity levels of both BERT models for all the intermediate MLP layers (plots a and b). We observe that both these models exhibit high levels of sparsity (< 10%) as other Transformer models. We further visualize the pre-activation values of the MLP layers as histograms in plots c and d. We observe that while they have mean 0 at initialization, the mean quickly becomes negative as training progresses, resulting in high sparsity levels.

**MLP-Mixer.** We evaluate the sparsity level of the MLP-Mixer [82], an all-MLP architecture constructed from cascading token-mixing and channel-mixing MLPs. Specifically, we use Mixer-B16 as the architecture, ADAM with  $\beta_1 = 0.9, \beta_2 = 0.999$  as the optimizer, and train on ImageNet-21k for 300 epochs. While [82] sweeps over a product set of hyper-parameters, here for simplicity we use a fixed set of hyper-parameters with weight decay of 0.03, gradient norm clipping at 1.0, base learning rate of 0.003, RandAugment magnitude of 10, no mixup, no stochastic depth, and no dropout.

Figure B.2 shows the sparsity level at the intermediate layer of both token mixing and channel mixing MLPs of Mixer-B16. We also plot the sparsity level of ViT (i.e., the plot in Figure 2a) to Figure B.2 for a comparison. It can be seen that the first four layers of channel mixing MLP and ViT have almost identical sparsity levels, while the rest of the layers (other than the last one) of channel mixing MLP are denser than the corresponding layer of ViT. On the other hand, the token mixing MLPs produce dense activation maps with more than 50% nonzero entries, probably because the dimension of the activation maps (384) is too small.

**Convolutional Neural Network (ConvNet).** Sparsity in activation maps has been studied for ConvNets such as the AlexNet [83] at least as early as in the work of [32]. There are also follow-up work [33, 34] on how enforcing sparse activation maps can help to gain computation efficiency. For completeness, we evaluate and present results for the sparsity level of residual networks (ResNets) [84], which is one of the most commonly used ConvNets, trained on ImageNet-1k. In particular, we focus on ResNet-18 and ResNet-50 which are constructed from stacking 8 standard residual blocks and 16 “bottleneck” residual blocks, respectively, where each block has two and three convolutional and ReLU layers, respectively. We examine the sparsity of activation maps after each of the ReLU layers in each residual block.

The results for ResNet-18 and ResNet-50 are reported in Figure B.3a and Figure B.3b, respectively. Here, the x-axis is the index of the residual block, and the sparsity of different layers in the residual blocks are plotted

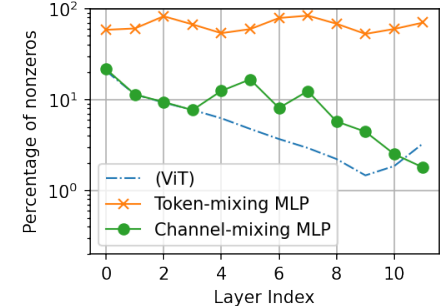


Figure B.2: Percentage of nonzero entries in activation maps of MLP-Mixer trained on ImageNet-21k. Results for token-mixing and channel-mixing MLPs are plotted in separate curves.

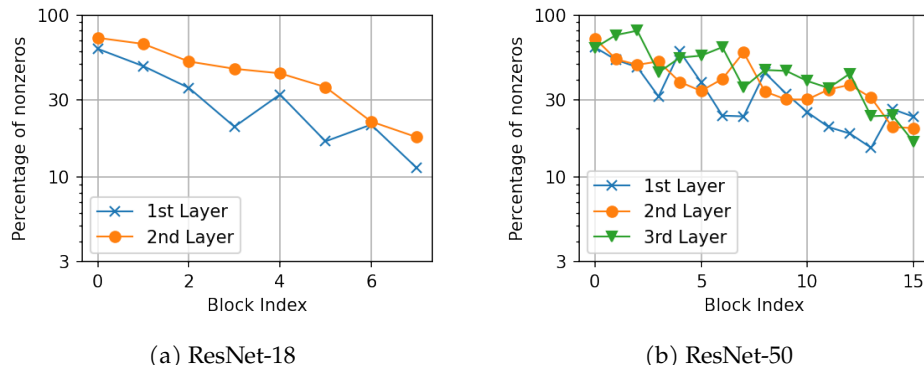


Figure B.3: Percentage of nonzero entries in activation maps of ResNet-18 and ResNet-50 trained on ImageNet-1k. Results for the two (resp., three) layers in each residual block (resp., bottleneck residual block) of ResNet-18 (resp., ResNet-50) are plotted in separate curves.

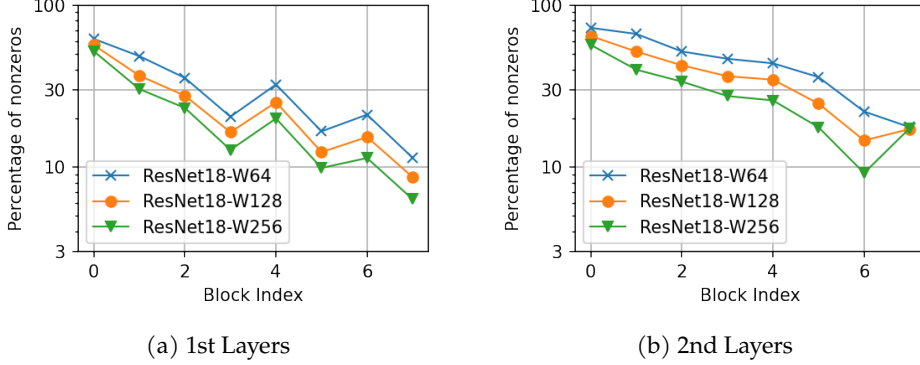


Figure B.4: Effect of network width  $\in \{64, 128, 256\}$  on sparsity level across layers of ResNet-18.

with separated curves in each figure. It can be observed that

- Layers near the network output tend to produce sparser activation maps than layers near the network input. This is aligned with the observation with ViT trained on ImageNet-1k (see Figure 2b).
- For each residual block, the intermediate layers (i.e., the 1st layer for ResNet-18 and the 1st & 2nd layers for ResNet-50) produce sparser activation maps than the output layer (i.e., 2nd layer for ResNet-18 and 3rd layer for ResNet-50).

In addition, all residual blocks are divided into four stages that have different output feature map sizes. For ResNet-50, the four stages are composed of blocks 0 - 2, 3 - 6, 7 - 12, and 13 - 15. Figure B.3b shows that there are patterns on how sparsity level varies within each stage and across the boundary of the stages.

- For the 1st layers, percentage of nonzeros decreases within each stage, and jumps up from the last layer of each stage to the first layer of next stage.
- For the 2nd layers, percentage of nonzeros decreases quickly at the beginning of each stage then becomes stable.
- For the 3rd layers, percentage of nonzeros tend to increase slightly within each stage, and jumps down from the last layer of each stage to the first layer of next stage.

Such observations may help to understand the role of each stage in ResNets.

Comparing the percentage of nonzero entries in ResNets (shown in Figure B.3a and Figure B.3b) and for Transformers (shown in Figure 2b), both of which are trained on ImageNet-1k, we see that ResNets produce much denser activation maps with more than 10% nonzero entries in all layers. Meanwhile, the trend that larger models are sparser for Transformers (see Section 2.2) holds for ResNets as well, as seen in Figure B.4. Here, we vary the width of ResNet-18 by multiplying the number of output channels of each convolutional layer by a factor of 1 (for width = 64), 2 (for width = 128), and 4 (for width = 256). The two subfigures show the effect of width on sparsity of the first and second layers in each residual block, respectively. In both cases, wider models have smaller percentage of nonzero entries across all layers, except for the very last layer (i.e., the 2nd layer in block #7 shown in Figure B.4b).

**Sparsity and Residual Learning.** We provide a study on the effect of residual connections on activation sparsity using T5. Each Transformer block contains two types of residual connections: the one that is in parallel with the attention blocks, and the one that is in parallel with the MLP blocks. We focus on the residual connection parallel to the MLP blocks. Towards that, we train two T5-Large models, one using the vanilla Transformer block and the other with residual connection removed for the Transformer block on encoder layer 6 (i.e., the 7<sup>th</sup> encoder layer, as we count from 0). There is a 1.6% evaluation accuracy drop with the latter model compared to the former model.

The percentage of nonzero entries of these two Transformers are presented in Figure B.5 for the encoder layers and in Figure B.6 for the decoder layers. It can be seen that in encoder layer 6 for which the residual connection is removed, the sparsity has a very different trend during training compared to the corresponding layer of the vanilla Transformer. Moreover, the sparsity level at all other layers also changes, though to a much smaller extend.

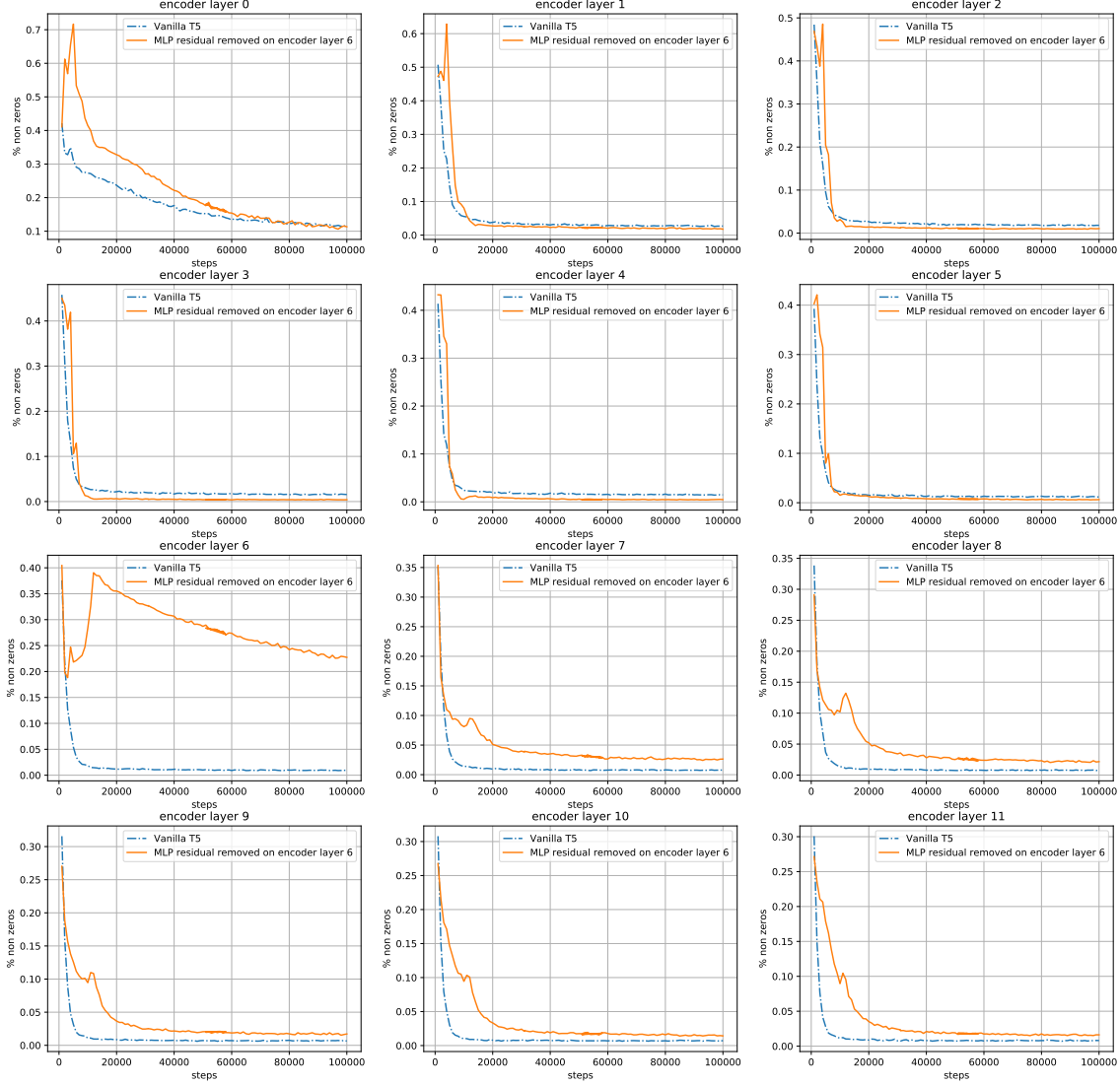


Figure B.5: Percentage of nonzero entries in activation maps in vanilla T5-Large and in a T5-Large with the residual connection parallel to MLP removed in the 7<sup>th</sup> encoder layer (i.e., encoder layer 6). Different subplots correspond to different *encoder* layers (see Figure B.6 for results on *decoder* layers). The encoder layer 6, which has its residual connection removed, shows a significant difference in both sparsity and the trend of sparsity during training. Sparsity level in other layers changes from vanilla T5-Large as well, though to a smaller extent.

## B.2 Sparsity and Optimizer

Transformers are usually trained using ADAM or its variants as the optimizer [80]. It may be curious to ask whether the emergence of sparsity is specific to such optimizers and whether other optimizers, such as stochastic gradient descent (SGD), also leads to sparse activation maps. However, we find that SGD cannot effectively train Transformer architectures such as T5 and ViT. Hence, we study the effect of optimizer on activation sparsity by looking at ResNet trained on ImageNet-1k following the setup in Section B.1, since both SGD and ADAM can effectively train the network. To train ResNet with ADAM, we use the same hyper-parameters as those used in SGD, with the only difference being that the optimizer is ADAM with  $\beta_1 = 0.9, \beta_2 = 0.999$ . To make the comparison with SGD fair, we tune the base learning rate for ADAM and select  $3e - 3$ , which is the one that gives the highest training accuracy among the set of  $\{1e - 4, 3e - 4, 1e - 3, 3e - 3, 1e - 2\}$ . The training accuracy obtained by ADAM with base learning rate  $3e - 3$  is similar to that obtained by SGD, namely,

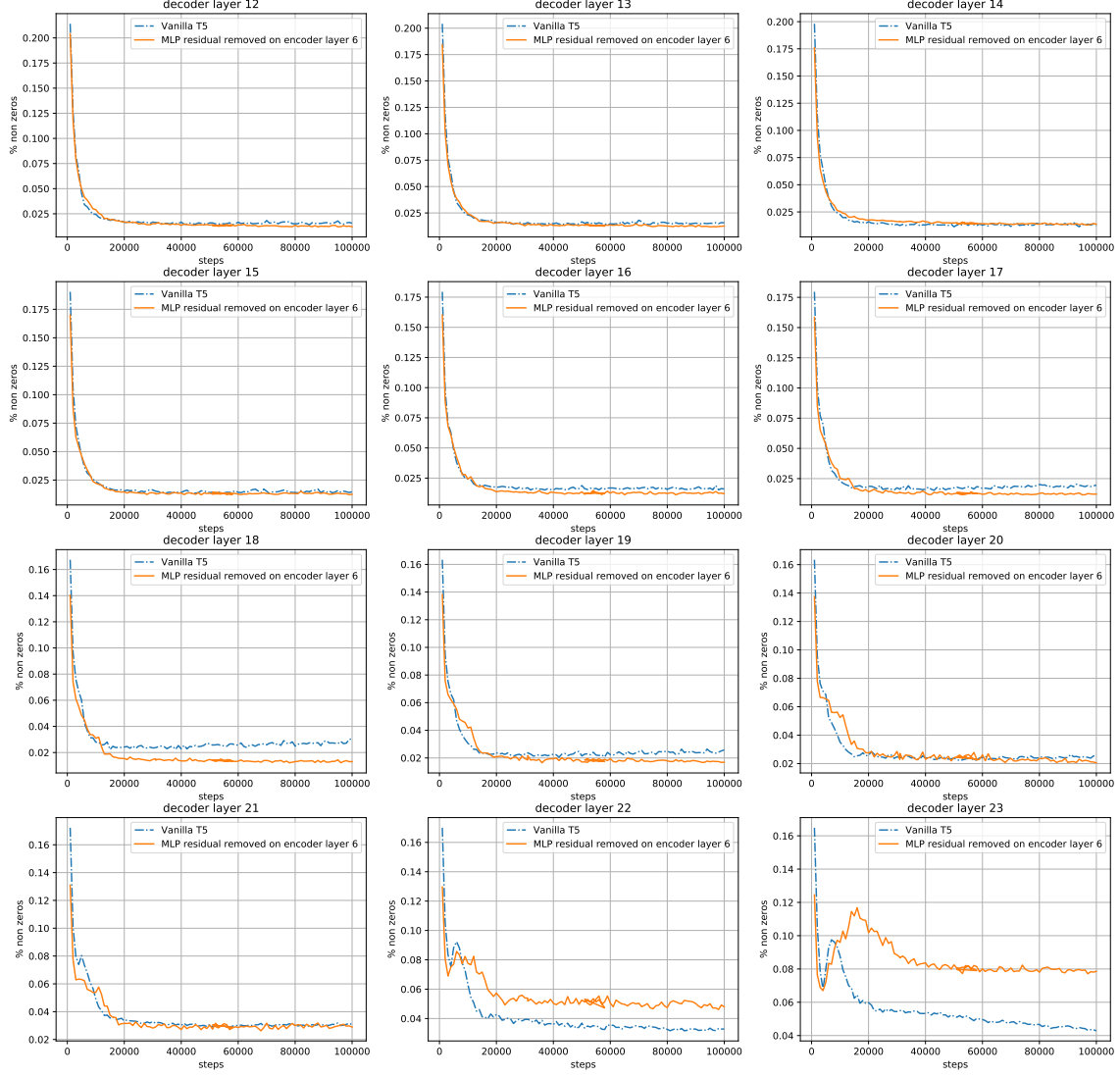


Figure B.6: Same setup as Figure B.5, but showing the results for the last 12 layers of the decoder.

67.8% by ADAM vs 69.3% by SGD with ResNet-18, and 75.0% by ADAM vs 78.5% by SGD with ResNet-50.

The results for ResNet-18 and ResNet-50 are presented in Figure B.7 and Figure B.8, respectively. For ResNet-18, we see that ADAM leads to a smaller percentage of nonzero entries particularly towards the output of the network for the first layers of each residual block. In contrast, ADAM and SGD have very similar sparsity level at the second layers of each residual block. Similar observation holds for ResNet-50, where the percentage of nonzero entries is smaller with ADAM for the first and second layers of each residual block, while for the third layer the sparsity level does not change much.

## C Additional Results on Benefits of Sparsity

### C.1 Benefits of Sparsity Persists with L1-Norm Induced Sparsity

While Top- $k$  thresholding is used in Section 4.3 to demonstrate the benefit of sparsity, we show that other means of obtaining sparsity, such as an explicit  $\ell_1$  norm regularization, also provides such benefits.

We experiment with ViT for ImageNet-1k classification under the same setup as in Section 4.3. Here instead of the Top- $k$  ViT, we train a regular ViT but with an additional loss term, which is the sum of the  $\ell_1$  norm of

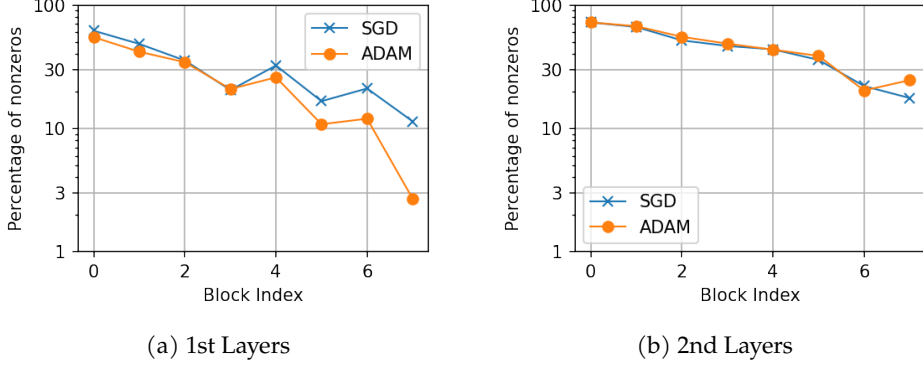


Figure B.7: Effect of optimizer on sparsity level across layers of ResNet-18.

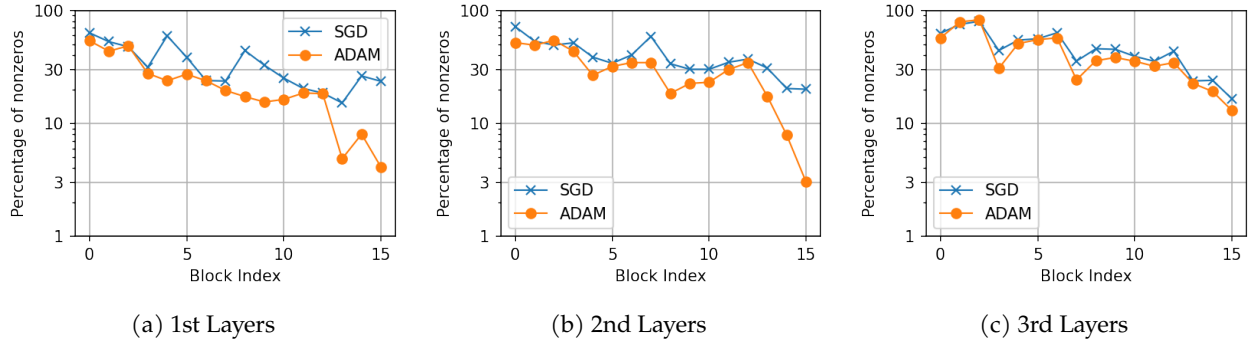


Figure B.8: Effect of optimizer on sparsity level across layers of ResNet-50.

all activation maps of ViT across all layers. We refer to the method as L1-ViT. We vary the weight  $\lambda$  on the  $\ell_1$  loss in the set  $\lambda \in \{0.01, 0.1, 1.0\}$  to control the strength of the regularization, and denote the corresponding methods as L1-ViT- $\{0.01, 0.1, 1.0\}$ .

The sparsity level, natural accuracy, robust accuracy under input perturbation, and ECE of L1-ViT are reported in Table C.1. We see that the averaged percentage of nonzero entries decreases with an increasing  $\lambda$ . With  $\lambda = 0.01$  or  $\lambda = 0.1$ , the robust accuracy and calibration all improves over ViT without hurting the natural accuracy. Using a  $\lambda = 1.0$  drastically reduces the percentage of nonzero entries and hurts the natural accuracy.

## C.2 Activation Regularization with L2 Norm

In addition to using  $\ell_1$  norm on the activation maps for enforcing sparsity, we also experiment with using  $\ell_2$  norm on the activation maps and report the results in Table C.2. It can be observed that  $\ell_2$  regularization also reduces the percentage of nonzero entries and improves performance in terms of robust accuracy under input perturbation and calibration error. However, the improvement in performance is less pronounced compared to those obtained with L1-ViT. For example, if we compare L1-ViT-0.01 and L2-ViT-0.1 which has similar sparsity level, the former one produces notably higher accuracy under input perturbation and lower ECE.

Conceptually, both  $\ell_1$  and  $\ell_2$  norm reduce the magnitude of entries in activation maps. The difference is that  $\ell_2$  norm penalizes more on entries with large magnitude, compared to the  $\ell_1$  norm which relatively focuses more on small entries. The fact that the benefit from  $\ell_2$  regularization is less prominent than  $\ell_1$  regularization indicates that the magnitude of large entries is less relevant for obtaining robustness and calibration. What matters more is whether the smaller entries can be suppressed or not.

Table C.1: Evaluation of ViT with a varying weights  $\in \{0.01, 0.1, 1.0\}$  on a  $\ell_1$  regularization upon activation maps for ImageNet-1k classification in terms of 1) averaged percentage of nonzero entries in activation maps across all layers, 2) natural accuracy (i.e., on ImageNet-1k evaluation set), 3) robust accuracy under input perturbation with additive {Gaussian, Impulse, Shot} noise, and 4) calibration error measured by ECE.

Methods	Avg. Perc. of Nonzeros	Natural Accuracy	Accuracy under Input Perturbation			Expected Calibration Error (ECE)
			Gaussian	Impulse	Shot	
ViT	5.67%	74.85%	39.54%	37.37%	38.56%	8.42%
L1-ViT-0.01	4.52%	74.98%	42.78%	41.11%	41.48%	6.86%
L1-ViT-0.1	3.34%	74.55%	41.90%	40.30%	40.44%	6.28%
L1-ViT-1.0	1.60%	73.21%	40.26%	38.01%	38.95%	6.34%

Table C.2: Same as Table C.1 but with  $\ell_1$  regularization replaced by  $\ell_2$  regularization of varying weights  $\in \{0.01, 0.1, 1.0\}$ .

Methods	Avg. Perc. of Nonzeros	Natural Accuracy	Accuracy under Input Perturbation			Expected Calibration Error (ECE)
			Gaussian	Impulse	Shot	
ViT	5.67%	74.85%	39.54%	37.37%	38.56%	8.42%
L2-ViT-0.01	5.22%	75.03%	41.26%	39.63%	40.03%	7.66%
L2-ViT-0.1	4.43%	74.67%	40.48%	38.51%	39.24%	7.64%
L2-ViT-1.0	3.08%	74.49%	40.76%	38.29%	39.37%	7.10%

## D Proof of Theorem 3.1

*Proof of Theorem 3.1.* For an arbitrary loss  $\ell(f(\mathbf{x}), \mathbf{y})$ , we have

$$\frac{\partial \ell}{\partial p_{i^*}} = \left\langle \frac{\partial \ell}{\partial f}, \frac{\partial f}{\partial p_{i^*}} \right\rangle = \left\langle \frac{\partial \ell}{\partial f}, \mathbf{v}_{i^*} \right\rangle. \quad (\text{D.1})$$

First, Consider  $\ell = \ell_{MSE}$ . We have

$$\frac{\partial \ell_{MSE}}{\partial f} = f(\mathbf{x}) - \mathbf{y} = \sum_i \sigma(p_i) \cdot \mathbf{v}_i - \mathbf{y}. \quad (\text{D.2})$$

Plugging this into (D.1), we obtain

$$\begin{aligned} \frac{\partial \ell_{MSE}}{\partial p_{i^*}} &= \left( \sum_i \sigma(p_i) \langle \mathbf{v}_i, \mathbf{v}_{i^*} \rangle \right) - \langle \mathbf{v}_{i^*}, \mathbf{y} \rangle \\ &= \left( \sum_{i \neq i^*} \sigma(p_i) \langle \mathbf{v}_i, \mathbf{v}_{i^*} \rangle \right) + \sigma(p_{i^*}) \langle \mathbf{v}_{i^*}, \mathbf{v}_{i^*} \rangle - \langle \mathbf{v}_{i^*}, \mathbf{y} \rangle \end{aligned} \quad (\text{D.3})$$

Taking the expectation, and noting the conditions in (4), we have

$$\mathbb{E} \left[ \frac{\partial \ell_{MSE}}{\partial p_{i^*}} \right] = 0 + \sigma(p_{i^*}) \mathbb{E} [\langle \mathbf{v}_{i^*}, \mathbf{v}_{i^*} \rangle] + 0 > 0. \quad (\text{D.4})$$

This finishes the proof for MSE loss.

In the rest of the proof we consider  $\ell = \ell_{CE}$ . We have

$$\frac{\partial \ell_{CE}}{\partial f} = \frac{\exp(f(\mathbf{x}))}{\langle \exp(f(\mathbf{x})), \mathbf{1} \rangle} - \mathbf{y} = \frac{\exp(\sum_i \sigma(p_i) \cdot \mathbf{v}_i)}{\langle \exp(\sum_i \sigma(p_i) \cdot \mathbf{v}_i), \mathbf{1} \rangle} - \mathbf{y}. \quad (\text{D.5})$$

Plugging this into (D.1), we obtain

$$\frac{\partial \ell_{CE}}{\partial p_{i^*}} = \frac{\langle \exp(\sum_i \sigma(p_i) \cdot \mathbf{v}_i), \mathbf{v}_{i^*} \rangle}{\langle \exp(\sum_i \sigma(p_i) \cdot \mathbf{v}_i), \mathbf{1} \rangle} - \langle \mathbf{v}_{i^*}, \mathbf{y} \rangle \quad (\text{D.6})$$

For the enumerator in the first term on the RHS of the equation above, we have

$$\begin{aligned} \left\langle \exp\left(\sum_i \sigma(p_i) \cdot \mathbf{v}_i\right), \mathbf{v}_{i^*} \right\rangle &= \sum_m \left( v_{i^*,m} \cdot \exp\left(\sum_i \sigma(p_i) \cdot v_{im}\right) \right) \\ &= \sum_m \left( v_{i^*,m} \cdot \exp(p_{i^*} \cdot v_{i^*,m}) \cdot \exp\left(\sum_{i \neq i^*} \sigma(p_i) \cdot v_{i,m}\right) \right) \end{aligned} \quad (\text{D.7})$$

Plugging this into (D.6) and denoting

$$C_m^{(1)} = \exp\left(\sum_{i \neq i^*} \sigma(p_i) \cdot v_{i,m}\right),$$

we obtain

$$\frac{\partial \ell_{CE}}{\partial p_{i^*}} = \sum_m \left( \frac{v_{i^*,m} \cdot \exp(p_{i^*} \cdot v_{i^*,m}) \cdot C_m^{(1)}}{\langle \exp(\sum_i \sigma(p_i) \cdot \mathbf{v}_i), \mathbf{1} \rangle} \right) - \langle \mathbf{v}_{i^*}, \mathbf{y} \rangle \quad (\text{D.8})$$

For the denominator in the first term on the RHS of the equation above, we have

$$\begin{aligned} \left\langle \exp\left(\sum_i \sigma(p_i) \cdot \mathbf{v}_i\right), \mathbf{1} \right\rangle &= \sum_{m'} \exp\left(\sum_i \sigma(p_i) \cdot v_{im'}\right) \\ &= \sum_{m'} \left( \exp(p_{i^*} \cdot v_{i^*,m'}) \cdot \exp\left(\sum_{i \neq i^*} \sigma(p_i) \cdot v_{im'}\right) \right) \\ &= \exp(p_{i^*} \cdot v_{i^*,m}) \cdot \exp\left(\sum_{i \neq i^*} \sigma(p_i) \cdot v_{i,m}\right) \\ &\quad + \sum_{m' \neq m} \left( \exp(p_{i^*} \cdot v_{i^*,m'}) \cdot \exp\left(\sum_{i \neq i^*} \sigma(p_i) \cdot v_{im'}\right) \right) \end{aligned} \quad (\text{D.9})$$

Plugging this into (D.8) and denoting

$$C_m^{(2)} = \exp\left(\sum_{i \neq i^*} \sigma(p_i) \cdot v_{i,m}\right), \quad (\text{D.10})$$

$$C_m^{(3)} = \sum_{m' \neq m} \left( \exp(p_{i^*} \cdot v_{i^*,m'}) \cdot \exp\left(\sum_{i \neq i^*} \sigma(p_i) \cdot v_{im'}\right) \right), \quad (\text{D.11})$$

we obtain

$$\frac{\partial \ell_{CE}}{\partial p_{i^*}} = \sum_m \left( \frac{v_{i^*,m} \cdot \exp(p_{i^*} \cdot v_{i^*,m}) \cdot C_m^{(1)}}{\exp(p_{i^*} \cdot v_{i^*,m}) \cdot C_m^{(2)} + C_m^{(3)}} \right) - \langle \mathbf{v}_{i^*}, \mathbf{y} \rangle. \quad (\text{D.12})$$

Taking expectation with respect to  $\mathbf{V}$  on both sides, and using the assumption that all entries of  $V$  are independent, we have

$$\begin{aligned}\mathbb{E}\left[\frac{\partial \ell_{CE}}{\partial p_{i^*}}\right] &= \sum_m \mathbb{E}\left[\frac{v_{i^*,m} \cdot \exp(p_{i^*} \cdot v_{i^*,m}) \cdot C_m^{(1)}}{\exp(p_{i^*} \cdot v_{i^*,m}) \cdot C_m^{(2)} + C_m^{(3)}}\right] - \mathbb{E}[\langle \mathbf{v}_{i^*}, \mathbf{y} \rangle] \\ &= \sum_m \mathbb{E}_{\{v_{i,l} | (i,l) \neq (i^*,m)\}} \left[ \mathbb{E}_{v_{i^*,m}} \left[ \frac{v_{i^*,m} \cdot \exp(p_{i^*} \cdot v_{i^*,m}) \cdot C_m^{(1)}}{\exp(p_{i^*} \cdot v_{i^*,m}) \cdot C_m^{(2)} + C_m^{(3)}} \right] \right] - \mathbb{E}[\langle \mathbf{v}_{i^*}, \mathbf{y} \rangle].\end{aligned}\quad (\text{D.13})$$

In above,  $\mathbb{E}_{v_{i^*,m}} \cdot \cdot \cdot$  means expectation with respect to  $v_{i^*,m}$ , and  $\mathbb{E}_{\{v_{i,l} | (i,l) \neq (i^*,m)\}} \cdot \cdot \cdot$  means expectation with respect to all other entries in  $\mathbf{V}$ . Note that  $C_m^{(1)}$ ,  $C_m^{(2)}$ , and  $C_m^{(3)}$  are independent of  $v_{i^*,m}$ . By Lemma D.1 and using the assumption that the expectation of  $\mathbf{V}$  is zero, we have

$$\mathbb{E}_{v_{i^*,m}} \left[ \frac{v_{i^*,m} \cdot \exp(p_{i^*} \cdot v_{i^*,m}) \cdot C_m^{(1)}}{\exp(p_{i^*} \cdot v_{i^*,m}) \cdot C_m^{(2)} + C_m^{(3)}} \right] > 0, \quad (\text{D.14})$$

and

$$\mathbb{E}[\langle \mathbf{v}_{i^*}, \mathbf{y} \rangle] = 0. \quad (\text{D.15})$$

Plugging the above two relations into (D.13), we obtain

$$\mathbb{E}\left[\frac{\partial \ell_{CE}}{\partial p_{i^*}}\right] > 0. \quad (\text{D.16})$$

□

The following lemma is used in the proof above.

**Lemma D.1.** *Let  $\mathbf{V}$  be a random variable with a probabilistic density function  $p(v)$  that satisfies  $P(\mathbf{V} = 0) \neq 1$ . Let  $C_1, C_2, C_3$  and  $p$  be positive numbers. Then,*

$$\mathbb{E}\left[\frac{C_1 \mathbf{V} \cdot \exp(p\mathbf{V})}{C_2 \exp(p\mathbf{V}) + C_3}\right] > \frac{C_1}{C_2 + C_3} \mathbb{E}[\mathbf{V}]. \quad (\text{D.17})$$

*Proof.* We may calculate the expectation by using the probabilistic density function  $p(v)$  as

$$\mathbb{E}\left[\frac{C_1 \mathbf{V} \cdot \exp(p\mathbf{V})}{C_2 \exp(p\mathbf{V}) + C_3}\right] = \mathbb{E}\left[\frac{C_1 \mathbf{V}}{C_2 + C_3 \exp(-p\mathbf{V})}\right] = \int_{-\infty}^{\infty} \frac{C_1 v}{C_2 + C_3 \exp(-pv)} p(v) dv \doteq \int_{-\infty}^{\infty} g(v) \cdot vp(v) dv. \quad (\text{D.18})$$

Since  $g(v)$  is monotonically increasing for  $v \in \mathbb{R}$ , we have  $g(v) \geq g(0)$  for  $v \geq 0$  and  $g(v) \leq g(0)$  for  $v \leq 0$ . Hence,

$$\int_{-\infty}^0 g(v) \cdot vp(v) dv \geq g(0) \int_{-\infty}^0 vp(v) dv, \quad (\text{D.19})$$

$$\int_0^{\infty} g(v) \cdot vp(v) dv \geq g(0) \int_0^{\infty} vp(v) dv. \quad (\text{D.20})$$

Moreover, since  $P(\mathbf{V} = 0) \neq 1$ , there exists an interval  $(a, b)$  such that  $\int_a^b p(v) dv > 0$ . Without loss of generality we assume that  $b > a \geq 0$ . Then,

$$\int_a^b g(v) \cdot vp(v) dv > g(0) \int_a^b vp(v) dv. \quad (\text{D.21})$$

That is, the inequality in (D.20) holds with strict inequality. Hence we have

$$\mathbb{E}\left[\frac{C_1 \mathbf{V} \cdot \exp(p\mathbf{V})}{C_2 \exp(p\mathbf{V}) + C_3}\right] = \int_{-\infty}^{\infty} g(v) \cdot vp(v) dv > g(0) \mathbb{E}[\mathbf{V}] = \frac{C_1}{C_2 + C_3} \mathbb{E}[\mathbf{V}]. \quad (\text{D.22})$$

□

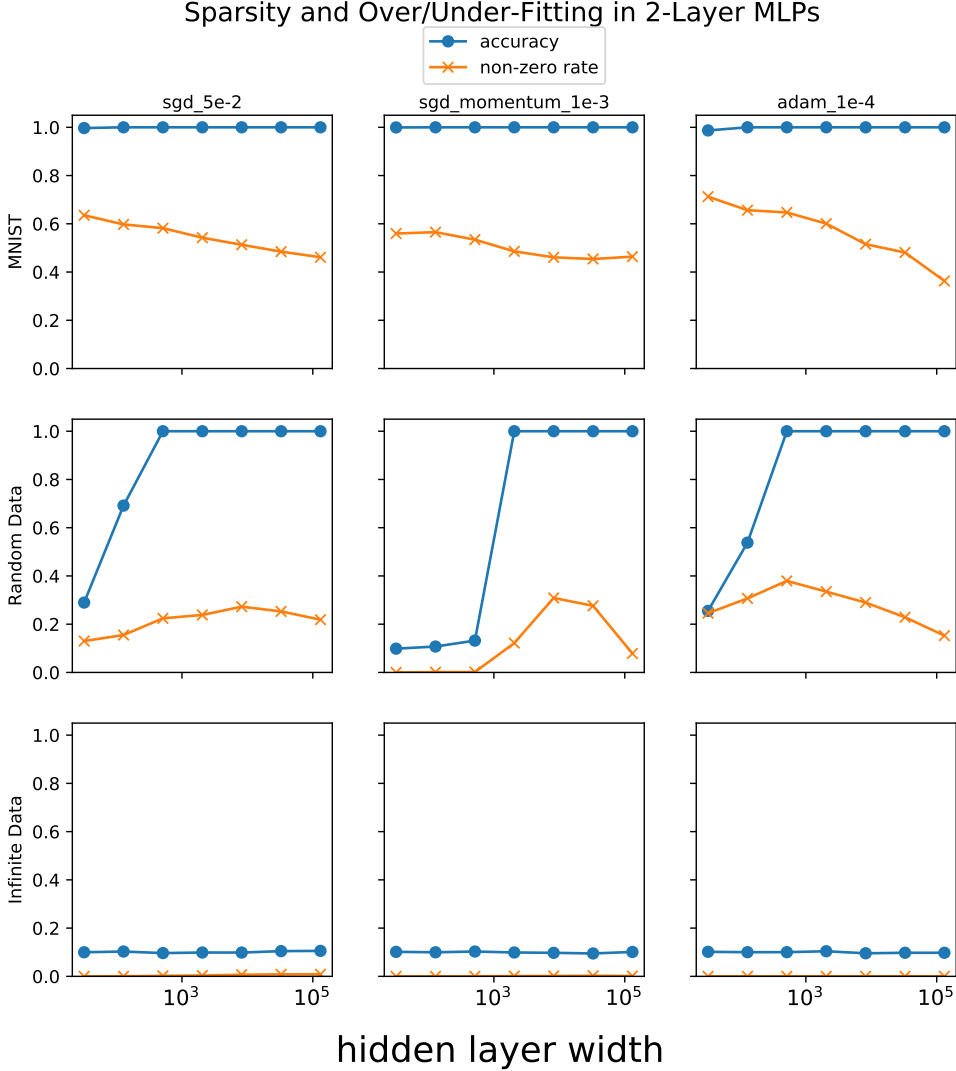


Figure E.1: Training accuracy and percentage of nonzero entries (both on the y-axis) in activation maps of two-layer MLPs of varying width (on the x-axis, in log scale) after 200 epochs of training. Rows correspond to different training datasets, and columns correspond to different training algorithms.

## E Insights from Sparsity in MLPs

We study the sparsity of activation maps in two-layer MLPs. By showing that sparsity emerges, the result here extends the scope of prevalence of activation sparsity from modern DNNs to two-layer MLPs which are one of the simplest neural network architectures. Moreover, by training such two-layer MLPs with different types of data, we provide additional insights on the causes for emergence of sparsity.

**Datasets.** We conduct our experiment with the MNIST dataset, which contains 60,000 grey scale images of handwritten digits. Similar to the experiment in Section 3, we also consider a dataset with *random* data, as well as a dataset with *infinite* data. For the random data, we replace each image of MNIST with a random one drawn from sampling i.i.d. pixels from uniform distribution, and each label with a random class amongst 10. Note that the image-label pairs are fixed throughout training. For the infinite data, the random images and random labels are generated on-the-fly, representing a random dataset of infinite size.

**Models and Training.** We train two-layer MLPs with ReLU activation maps with varying width (i.e., hidden dimension): 32, 128, 512, 2048, 8192, 32768 and 131072. We use three different optimizers: SGD, SGD with momentum, and Adam, all for 200 epochs (for the infinite data case, we use the same number of iterations as that for training on MNIST and random data). We find that 200 epochs is sufficient for the reported metrics to converge in most of the cases.

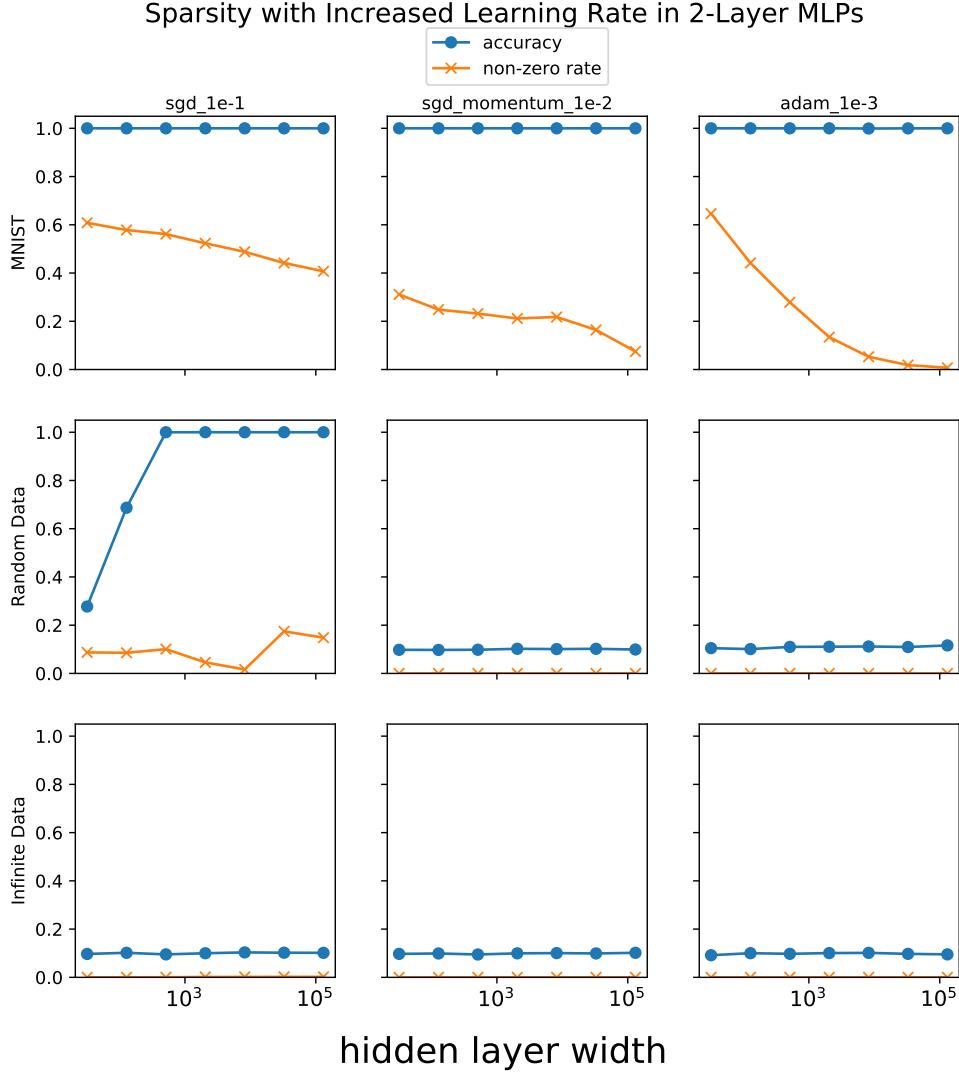


Figure E.2: The same as in E.1 except that for each optimizer we use a larger learning rate.

**Results.** We report training accuracy and the percentage of nonzero entries in the intermediate activation map (i.e., non-zero rate) at the end of the training in Figure E.1. We have the following observations.

- For random data, we observe a *uni-modal* shaped curve for sparsity level. Namely, when the model width is small hence the model cannot well-fit the training data, the percentage of nonzero entries is small. As the model width increases, where the model is able to fit the training data evidenced by the fact that the training accuracy increases, we observe that the percentage of nonzero entries starts to increase. However, as we further increase the model size in the regime where model is able to perfectly fit the training data, we see that the percentage of nonzeros starts to decrease.
- For infinite data, where the model cannot fit the training data (hence training accuracy is 0.1 which is the

same as result from random guessing), the percentage of nonzero entries is close to 0. This is aligned with the result of random data experiment with a small model width.

- For MNIST, where the model of varying width in our experiment is able to fit the training data, we observe that the percentage of nonzero entries decreases. This trend aligns with the random data experiment with large model width

The evidence above suggest that the sparsity level may be associated with the under- and over-parameterization of the models. Namely, the percentage of nonzero entries is the highest when the model size is close to the point that the model can start to fit the training data (i.e., the interpolation threshold), and is lower in both under and over-parameterized regimes. It may be intriguing to note that a similar pattern exists for the variance (as in the bias-variance tradeoff) curve of deep learning models, which as shown in [70] to exhibit a uni-modal shape as well. Such a connection may help us understand the interplay between generalization and sparsity of activation in deep learning models.

Finally, in Figure E.2 we report the results obtained with optimizers with larger learning rates compared to those used in Figure E.1. It can be observed that larger learning rate produces sparser activation maps.